Robust Energy Management System Based on Interval Fuzzy Models

Felipe Valencia, *Member, IEEE*, Doris Sáez, *Senior Member, IEEE*, Jorge Collado, Fernanda Ávila, Alejandro Marquez, and Jairo J. Espinosa, *Senior Member, IEEE*

***Abstract*— Energy management systems (EMSs) are used for operators to optimize, monitor, and control the performance of a power system. In microgrids, the EMS automatically coordinates the energy sources aiming to supply the demand. The coordination is carried out considering the operating costs, the available energy, and the generation and transmission capabilities of the grid. With this purpose, the available energy of the sources is predicted, and the operating costs are minimized. Thereby, an optimal operation of the microgrid is achieved. Often, the optimization procedure is executed throughout a receding horizon (model predictive control approach). Such approach provides some robustness to the microgrid operation. But, the high variability of the nonconventional energy sources makes the prediction task very complex. As a consequence, the reliable operation of the microgrid is compromised. In this paper, a scenario-based robust EMS is proposed. The scenarios are generated by means of fuzzy interval models. These models are used for solar power, wind power, and load forecasting. Since interval fuzzy models provide a range rather than a trajectory, upper and lower boundaries for these variables are obtained. Such boundaries are used to formulate the EMS as a robust optimization problem. In this sense, the solution obtained is robust against any realization of the uncertain variables inside the intervals defined by the fuzzy models. In addition, the original robust optimization problem is transformed into an equivalent second-order cone programming problem. Hence, desired mathematical properties such as the convexity of the optimization problem might be guaranteed. Therefore, efficient algorithms, based, e.g., on interior-point methods, could be applied to compute its solution. The proposed EMS is tested in the microgrid installed in Huatacondo, a settlement located at the north of Chile.**

***Index Terms*— Energy management systems (EMSs), interval fuzzy models (INFUMOs), microgrids, model predictive control (MPC), robust optimization.**

I. Introduction

MICROGRIDS have received much attention in recent years due to their widely recognized capabilities in the integration of distributed generation, such as photovoltaic and wind-based generation. Likewise, since distributed generation shortens the distance between the generation and load centers, microgrids help to increase the efficiency of power systems. According to [1], a microgrid is a low voltage grid with a nominal capacity of around ten kilowatts, composed mainly by loads, nonconventional energy sources (NCES), storage systems, and a distribution grid. The operation of a microgrid commonly has a hierarchical structure including [2] the following:

1) a relatively fast primary voltage and frequency control in each energy source (often including a droop loop to share the active and reactive power between the units);
2) a slower secondary control loop to restore the frequency and the voltage of the overall system;
3) a tertiary control or energy management system (EMS), used to achieve reliable and cost-effective operation of microgrids by the dispatch and commitment of the available generation units.

In general, primary and secondary control loops are implemented using classic control schemes such as proportional–integral controllers, while the tertiary control loop is implemented using optimization-based control techniques. As it can be observed, the coordination among energy sources is carried out in the tertiary control level. At this level, the most cost-effective combination of generation units to meet the predicted load and reserve requirements is defined [3]. This paper focuses on the tertiary control of microgrids. Microgrids have many uses in the energy field [5], for example, as an alternative for electrifying isolated settlements; the case analyzedin this paper. However, the uncertain nature of the NCES makes that the use of a tertiary control does not guarantee a reliable operation of a microgrid. One way to cope with the uncertainty of the NCES is the use of energy storage systems (ESSs). The use of ESS allows including the NCES in the tertiary control as dispatchable energy sources. But, exploiting the benefits of the ESS requires the proper

Manuscript received August 28, 2014; revised January 30, 2015; accepted February 15, 2015. Date of publication April 30, 2015; date of current version December 21, 2015. Manuscript received in final form March 10, 2015. This work was supported in part by the Solar Energy Research Center SERC-Chile, CONICYT/FONDAP/ Project under Grant 15110019; in part by the National Fund for Science and Technology Project under Grant 1140775; and Complex Engineering Systems Institute (ICM: P-05-004-F, CONICYT: FBO16). Recommended by Associate Editor B. Pal.

F. Valencia, D. Sáez, J. Collado, and F. Ávila are with the Department of Electrical Engineering, Solar Energy Research Center SERC-Chile, Faculty of Physical and Mathematical Sciences, University of Chile, Santiago 8370451, Chile (e-mail: felipe.valencia@sercchile.com; dsaez@ing.uchile.cl; jcollado1111@gmail.com; favila@ing.uchile.cl).

A. Marquez and J. J. Espinosa are with the Department of Engineering and Automation, Universidad Nacional de Colombia, Medellin CO 050041, Colombia (e-mail: amarque@unal.edu.co; jairo.espinosa@ieee.org).

Color versions of one or more of the figures in this paper are available online at http://ieeexplore.ieee.org.

Digital Object Identifier 10.1109/TCST.2015.2421334

design of an EMS since its performance depends upon: 1) the prediction of the available energy in the NCES and 2) the prediction of the load.

In the past decades, several optimization methods with application to management and decision making under uncertainty have been reported in the specialized literature (see [6], [7], and the references therein). In [6] and [8]–[10], these approaches have been classified as fuzzy, stochastic, and mathematical programming. Following this classification, fuzzy and mathematical programming problems have been formulated considering robust programming as mathematical framework. Robust programming is a class of optimization problem where the parameters and/or constraints are uncertain and prescribed into a defined set [11]. Thus, the following conditions hold:

1) The use of probability density functions (pdfs) is not required, i.e., only the mean value and the range of the uncertain data is required.
2) The solution is robust against all realizations of the uncertain data within a deterministic uncertain set [7].

In stochastic programming, several realizations of the uncertain variables are considered. Each realization has a probability of occurrence. Depending on this probability, a robust solution is obtained.

Among the identified alternatives, Wang *et al.* [6], Wang and Huang [8], [9], and Nie *et al.* [10] investigated the use of two-stage stochastic fuzzy programming for supporting water resource management, for flood-diversion planning, and for municipal solid waste management under uncertainty. In two-stage stochastic fuzzy programming, an initial decision is made considering a deterministic scenario. Then a second decision is made considering a realization of the uncertain variables. In the aforementioned references, interval-valued membership functions were used to represent the uncertainty. Thus, upper and lower values for the uncertain variables were obtained. Given these values, the first decision was made. Then, a feasibility test was performed to eliminate the unfeasible solutions. Finally, the second decision was made over the feasible solutions. At the end of the process, a set of solutions was obtained.

In large-scale power systems, similar approaches have also been reported. For example, in [7], [12], and [13], multistage optimization-based methodologies were proposed for solving the unit commitment considering wind-based generation and price responsive demand and for dealing with the home energy management demand problem. In [7] and [12], the first decision stage consisted in the unit commitment. The second decision stage consisted in the power dispatch. Only in [12], a third decision stage was added. The additional stage included the uncertainty in the price-elastic demand curve. In [13], the optimization problem was separated according to the different time scales of the system response. Specifically, slow (hours) and fast (minutes) scales were considered. Moreover, only uncertainty was included in the solution of the optimization problem associated with the fast dynamics. Such an optimization problem was solved using a stochastic programming technique. Neither in [7] and [12] nor in [13], fuzzy models were used to represent the uncertainty. Indeed, in [12], time-independent intervals were proposed.

With regard to microgrid applications, model predictive control (MPC) arises as an alternative for dealing with the uncertainty [4], [5], [14], [15]. In this framework, the optimization problem is solved through a prediction horizon. Then, a sequence of units dispatch is obtained. The first element of such a sequence is applied and the remaining elements are used as the initial condition for the solution at the next time step. In [4] and [14], neither the uncertainty of the NCES nor the uncertainty of the load was considered. By contrast, Zhang *et al.* [5] and Zhao *et al.* [15] proposed two different robust EMS approaches, namely, one based on robust programming and another one based on stochastic programming. Unlike the methods reported in the literature for large-scale power systems, the approaches in [5] and [15] only required the solution of a single optimization problem. However, in [5], time-independent intervals were considered to represent the uncertainty of the NCES (as in [12]), and in [15], pdfs were used to represent the uncertainty. Therefore, the solution in [5] could be very conservative and the solution in [15] was only robust against the realizations considered in the formulation.

Notwithstanding the success of robust optimization in management and decision making and, in particular, considering the amount of applications developed for large-scale power systems, little attention has been paid to the combined use of fuzzy interval models and robust programming to formulate a robust predictive EMS. Until the literature review allowed us to know, only in [16], a fuzzy inference model was used in an EMS to determine the forecasting conditions, based on the historical values of the prediction error. In this approach, the power was classified as low, medium, and high. The cutoff risk was also sorted out as no cutoff and cutoff risk. Based on the aforementioned classifications, a probability of occurrence was associated with the resulting sets of prediction errors. In this way, the uncertainty in the prediction was included in the optimization problem. This paper presents a robust predictive EMS, where the predictions are carried out by means of interval fuzzy models (INFUMOs). Those models allowed handling the uncertainty present in the NCES and in the load. In accordance with [17], INFUMOs are fuzzy models whose output is an interval instead of a trajectory. The width of the interval is determined by the desired confidence level, or coverage probability, for representing the uncertainty in the modeled phenomena. Thus, given a set of inputs, the INFUMO provides upper and lower boundaries for the trajectory of the phenomena under study. In contrast with the interval-valued membership functions used in [6] and [8]–[10], the INFUMO uses single-valued membership functions. Consequently, the amount of data required for the parameter identification is slightly diminished. Furthermore, the use of single-valued membership functions also decreases the complexity of the model, without compromising its ability to represent the uncertainty.

In particular, in this paper, INFUMOs are used to predict the trajectories of the solar power, the wind power, and the load. Given the upper and lower boundaries for these variables,

different scenarios are generated. The scenarios come from all possible combinations of the trajectories provided by interval model (eight scenarios in total). With the already defined scenarios, the dispatch in a microgrid is formulated as a robust programming problem. Note that each scenario defines a possible power balance. Since unfeasible solutions might arise, an additional term associated with the unserved power is included in the cost function (as in [4]). Moreover, a slack variable is also considered to relax the power flow equality constraint. The use of an additional term and a slack variable is motivated by the fact that in isolated microgrids, the power balance is not always satisfied.

With the combination of both INFUMOs and robust programming, and following the procedure in [11], the original robust dispatch problem is transformed in an equivalent second-order cone programming (SOCP) problem. Since SOCP problems are convex, the solution can be efficiently computed by means of, e.g., interior-point methods. Furthermore, the convergence of the solution to the global optimum might be guaranteed. In comparison with the multistage approaches previously described, the proposed robust EMS requires the solution of a single optimization problem. Moreover, with regard to the approaches in [4] and [14], the proposed robust EMS includes the uncertainty associated with the NCES and the load forecasting. Finally, with respect to the approach in [5], the time dependency of the uncertainty is considered in this paper. Such a dependency is given by the dynamics of the system, which is here represented by the INFUMO. Hence, the interval is wider where the historical data exhibited more variability than where the historical data exhibited less variability. This provides an enhanced representation of the uncertainty and reduces the conservativeness of the robust solution.

The remainder of this paper is organized as follows. In Section II, the robust predictive control based on scenarios is described. With this aim, the INFUMO is introduced and the scenarios arising from the use of the INFUMO are explained. In Section III, the formulation of the EMS as a robust predictive control based on scenarios is presented. Finally, Sections IV and V gather the simulations results and concluding remarks. In this paper, the microgrid installed in Huatacondo, north of Chile, was used to evaluate the performance of the proposed robust EMS.

II. Robust Predictive Control Based on Interval Fuzzy Models

A. Scenario-Based Robust Predictive Control

Consider an optimization problem where the objective is to minimize the cost function $J(x) = \|Ax - b\|$. Let $A \in \mathbb{R}^{m\times n}$, $x \in \mathbb{R}^{n\times 1}$, and $b \in \mathbb{R}^{m\times 1}$, where A and/or b are the random variables with a pdf describing their variations. Such an optimization problem recasts in the minimization of the expected value of $J(x)$. Thus, it becomes in an expected value problem whose solution depends on the uncertainty description. In fact, in many applications, the resulting optimization problem is not tractable. For this reason, uncertainty description by means of polytopes or norm-bounded models is proposed in the literature (see [18] for details).

An specific case where the expected value problem is solvable is the worst case problem (WCP). In WCP, the uncertainty is described by a set of possible values for A and b. Given these values and assuming the worst conditions for the uncertainty, the value of x minimizing $J(x)$ is computed. Thereby, the expected value becomes a min–max optimization problem. The WCP have been widely studied in [19]–[23]. But notwithstanding its advantages, often WCP belongs to robust nonlinear programming (RNLP) problems. With the present computation resources, it is almost impossible to find the exact solution of RNLP problems in real time [24]. Then, in general, linear approximations of the system dynamics are used in robust control applications. In this way, the complexity of WCP is significantly reduced.

At time step k, let $x(k) \in \mathbb{R}^n$, $u(k) \in \mathbb{R}^m$, and $y(k) \in \mathbb{R}^z$ denote the states, inputs, and outputs of a given system, respectively. Let $\widetilde{x}(k) = [x^T(k), \ldots, x^T(k+N_p)]^T$ and $\widetilde{u}(k) = [u^T(k), \ldots, u^T(k+N_u)]^T$, with N_p and N_u the prediction and control horizons, respectively [often the constraint $u(k+j) = u(k+N_u)$, $N_u \le j \le N_p$, is added for extending $\widetilde{u}(k)$ along N_p, i.e., $\widetilde{u}(k) = [u^T(k), \ldots, u^T(k+N_p-1)]^T$]. Let $\tilde{\hat{y}}(k) = [\hat{y}^T(k+1), \ldots, \hat{y}^T(k+N_p)]^T$ and $\tilde{y}_{\text{ref}}(k) = [y_{\text{ref}}^T(k+1), \ldots, y_{\text{ref}}^T(k+N_p)]^T$ denote the predicted outputs of the system and the reference for the controller, respectively. Then assuming a linear approximation of the system dynamics, $\tilde{\hat{y}}(k)$ is given by

$$\tilde{\hat{y}}(k) = \Gamma + \Lambda\widetilde{u}(k)$$

where Γ and Λ are, respectively, the matrices defining the free and forced responses of the linear system throughout N_p [24], [25].

Since a linear approximation is being used, uncertainties in both the free and forced responses of the system appear. In fact, as the system moves away from the equilibrium point used in the linearization, the uncertainties increase. Let $\delta\Gamma$ and $\delta\Lambda$, respectively, denote the uncertainties in free and forced response of the system. Then $\tilde{\hat{y}}(k)$ becomes

$$\tilde{\hat{y}}(k) = (\Gamma + \delta\Gamma) + (\Lambda + \delta\Lambda)\widetilde{u}(k). \tag{1}$$

Assume that $J(y_{\text{ref}}(k+l), \hat{y}(k+l), u(k+l), \delta\Gamma, \delta\Lambda)$ is a quadratic function given by

$$\begin{aligned} &J(y_{\text{ref}}(k+l), \hat{y}(k+l), u(k+l), \delta\Gamma, \delta\Lambda) \\ &\quad= \sum_{l=1}^{N_p} \|y_{\text{ref}}(k+l) - \hat{y}(k+l)\|_Q^2 \\ &\qquad+ \sum_{l=1}^{N_p} \|u(k+l)\|_R^2 + \sum_{l=1}^{N_p} \|\Delta_u u(k+l)\|_S^2 \end{aligned} \tag{2}$$

with Q, R, and S the positive definite diagonal matrices, and with $\Delta_u\widetilde{u}(k)$ the difference between the actual and the previous value of the control action. The cost function (2) penalizes the deviation of $\hat{y}(k)$ from $y_{\text{ref}}(k)$, the magnitude of the control actions, and the changes in the control actions. The following quadratic form for $J(y_{\text{ref}}(k+l), \hat{y}(k+l),$

$u(k+l), \delta\Gamma, \delta\Lambda)$ is obtained by replacing (1) into (2):

$$J(y_{\text{ref}}(k+l), \hat{y}(k+l), u(k+l), \delta\Gamma, \delta\Lambda) = r + q\widetilde{u}(k) + \widetilde{u}^T(k) P \widetilde{u} k \quad (3)$$

where

$$\begin{aligned} P &= \Lambda^T Q \Lambda + \Lambda^T Q \delta\Lambda + \delta\Lambda^T Q \Lambda \\ &\quad + \delta\Lambda^T Q \delta\Lambda + R + \Delta_u^T S \Delta_u \\ q &= (\Gamma - \tilde{y}_{\text{ref}}(k))^T Q \Lambda + (\Gamma - \tilde{y}_{\text{ref}}(k))^T Q \delta\Lambda \\ &\quad + \delta\Gamma^T Q(\Lambda + \delta\Lambda) - \overline{u}(k-1)^T S \Delta_u \\ r &= J_{\min} + \Gamma^T Q \delta\Gamma + \delta\Gamma^T Q \Gamma + \delta\Gamma^T Q \delta\Gamma \\ J_{\min} &= \tilde{y}_{\text{ref}}(k)^T Q \tilde{y}_{\text{ref}}(k) + \Gamma^T Q \Gamma - 2\tilde{y}_{\text{ref}}(k)^T Q \Gamma \\ &\quad + \overline{u}(k-1)^T S \overline{u}(k-1). \end{aligned}$$

In (3), $\overline{u}(k-1) = [u^T(k-1), 0^T]^T$. Note that $P = \overline{P} + \delta P$, $q = \overline{q} + \delta q$, and $r = \overline{r} + \delta r$, with $\overline{P} = \Lambda^T Q \Lambda + R + \Delta_u^T S \Delta_u$, $\overline{q} = (\Gamma - \tilde{y}_{\text{ref}}(k))^T Q \Lambda - \overline{u}(k-1)^T S \Delta_u$, $\overline{r} = J_{\min}$, $\delta P = \Lambda^T Q \delta\Lambda + \delta\Lambda^T Q \Lambda + \delta\Lambda^T Q \delta\Lambda$, $\delta q = (\Gamma - \tilde{y}_{\text{ref}}(k))^T Q \delta\Lambda + \delta\Gamma^T Q(\Lambda + \delta\Lambda)$, and $\delta r = \Gamma^T Q \delta\Gamma + \delta\Gamma^T Q \Gamma + \delta\Gamma^T Q \delta\Gamma$. Hence, there is a mapping from the model to the uncertainty in the parameters of $J(y_{\text{ref}}(k+l), \hat{y}(k+l), u(k+l), \delta\Gamma, \delta\Lambda)$. Specifically, associated with each pair $(\delta\Gamma, \delta\Lambda)$, there exists a tuple $(\delta P, \delta q, \delta r)$ and therefore a tuple (P, q, r).

Let $\Theta_\Gamma := \{\delta\Gamma_1, \ldots, \delta\Gamma_M\}$ and $\Theta_\Lambda := \{\delta\Lambda_1, \ldots, \delta\Lambda_M\}$. Then, the set of tuples

$$\mathbb{T} := \{(P_1, q_1, r_1, \Gamma_1, \Lambda_1), \ldots, (P_M, q_M, r_M, \Gamma_M, \Lambda_M)\} \quad (4)$$

defines all the possible scenarios arising from Θ_Γ and Θ_Λ i.e., $\mathbb{T}$ includes all realizations of Γ and Λ. (In this paper, these values are generated by means of the INFUMO. A detailed description is provided in Section II-C.) Let $\mathbb{F}$ denote the set of tuples (P_i, q_i, r_i), $i = 1, \ldots, M$, coming from Θ_Γ and Θ_Λ. That is, $\mathbb{F} := \{(P_1, q_1, r_1), \ldots, (P_M, q_M, r_M)\}$. In accordance with [11], the associated worst case error $e_{\text{wc}}(\widetilde{u}(k))$ of a candidate approximate solution $\widetilde{u}(k)$ is given by

$$e_{\text{wc}}(\widetilde{u}(k)) := \sup_{(P,q,r,\Gamma,\Lambda)} \left\{ \widetilde{u}^T(k) P \widetilde{u}(k) + 2q\widetilde{u}(k) + r \mid (P, q, r) \in \mathbf{conv}\{\mathbb{F}\} \right\} \quad (5)$$

where $\mathbf{conv}\{\mathbb{F}\}$ denotes the convex hull of $\mathbb{F}$. Recall that $\overline{P} = \Lambda^T Q \Lambda + R + \Delta_u^T S \Delta_u$. Since $\delta\Gamma$ and $\delta\Lambda$ have associated different values of Γ and Λ, P_i, $i = 1, \ldots, M$ is symmetric. Therefore, $\widetilde{u}^T(k) P_i \widetilde{u}(k) = \|P_i^{(1/2)} \widetilde{u}(k)\|_2$. Following the procedure presented in [11], scenario-based RMPC can be written as the epigraph minimization problem:

$$\begin{aligned} &\min_{\widetilde{u}(k), t, f} \quad t + f \\ &\text{s.t.} \left\| P_i^{\frac{1}{2}} \widetilde{u}(k) \right\|_2 \le t \\ &t + 2q_i \widetilde{u}(k) + r_i \le f \\ &\begin{bmatrix} I \\ -I \\ \Delta_u \\ \Delta_u \\ \Lambda_i \\ -\Lambda_i \end{bmatrix} \widetilde{u}(k) \le \begin{bmatrix} \tilde{u}_{\max} \\ -\tilde{u}_{\min} \\ \tilde{\Delta u}_{\max} + \overline{u}(k-1) \\ \tilde{\Delta u}_{\max} - \overline{u}(k-1) \\ \tilde{y}_{\max} - \Gamma_i \\ -\tilde{y}_{\min} + \Gamma_i \end{bmatrix}. \end{aligned} \quad (6)$$

Note that the minimization problem (6) includes the intrinsic uncertainty of linear models. Nevertheless, its solution might result conservative since the system is not always operating at the worst case conditions. Furthermore, how conservative is the solution of (6) depends on the selection (or definition) of the sets Θ_Γ and Θ_Λ. For dealing with these disadvantages, in this paper, INFUMOs are proposed as prediction model. Being that the INFUMO provides an interval rather than a system trajectory, the uncertainty is accurately characterized. Consequently, it is expected that the solution of (6) is less conservative. In the next section, INFUMOs are introduced and briefly explained.

B. Interval Fuzzy Models

Often, system modeling regards the reconstruction of state and/or output specific paths. However, in the presence of large uncertainties having a range could be more useful than having an specific trajectory. Indeed, if the range is designed in such a way that the dynamic behaviors of the states and/or outputs of the system are represented. Then system dynamics and system uncertainties are both included in a single model. In accordance with [17], the aforementioned procedure is called interval modeling. In this procedure, families of functions are approximated given a finite set of input and output measurements. The approximation is carried out considering a confidence level. Given the desired confidence level, the width of the interval is determined.

There are two considerations in interval modeling [17].

1) The interval model should be identified with a confidence band as narrow as possible.
2) The resulting model should also generate a band that contains a high percentage of the data.

In the literature, several interval modeling approaches have been proposed [26]–[29]. Mainly, they are based on a multimodel representation of the system. The use of a single or multiple models depends on the degree of uncertainty and/or the strength of the nonlinearity of the system. For instance, Škrjanc *et al.* [17] proposed the use of Takagi–Sugeno (TS) models, which belong to multimodel approaches. The reason for the selection of TS models lies in the fact that they are able to approximate a large class of nonlinear systems, despite the type of nonlinearity [30].

At time step k, let $x_p(k)$, and $x(k)$, respectively, denote the vectors of premises and consequences in a TS model. Let $z(k) = [x_p^T(k), x^T(k)]^T$ denote the vector of input variables, and $\beta_j(x_p(k))$ be the normalized activation degree of the jth rule. The normalized activation degree satisfies $\beta_j(x_p(k)) >= 0$, $j = 1, \ldots, M_{\text{TS}}$, $\sum_{j=1}^{M_{\text{TS}}} \beta_j(x_p(k)) = 1$, M_{TS} being the number of rules, whereby depending on its fulfillment, $\beta_j(x_p(k))$ assigns a value between zero and one to the consequence of the jth rule. Let θ_j denote the vector of parameters of the linear model associated with the consequence of the jth rule. Then, in accordance with [17], the output of a TS model is given by

$$\hat{y}(k) = \sum_{j=1}^{M_{\text{TS}}} \beta_j(x_p(k)) \theta_j^T x(k). \quad (7)$$

The objective of interval modeling is to find the upper and lower boundary functions $\overline{f}(z(k))$ and $\underline{f}(z(k))$, such that

$\underline{f}(z(k)) \le y(k) \le \overline{f}(z(k))$ (here the inequality indicates an element-to-element relationship). Assume that $f(z(k))$ has the form: $f(z(k)) = \sum_{j=1}^{M_{\mathrm{TS}}} \beta_j(x_p(k))\theta_j^T x(k)$. Then the vectors $\overline{\theta}_j$ and $\underline{\theta}_j$ define the upper and lower boundaries of $f(z(k))$, respectively. The values of $\overline{\theta}_j$ and θ_j are obtained by solving optimization problems [17]

$$\begin{aligned}&\min_{\underline{\theta}_j}\max_i \quad \left\{|y_i(k) - \sum_{j=1}^{M_{\mathrm{TS}}} \beta_j(x_p(k))\underline{\theta}_j^T x(k)|\right\}\\ &\text{s.t.} \quad y_i(k) - \sum_{j=1}^{M_{\mathrm{TS}}} \beta_j(x_p(k))\underline{\theta}_j^T x(k) \ge 0 \end{aligned} \tag{8}$$

$$\begin{aligned}&\min_{\overline{\theta}_j}\max_i \quad \left\{|y_i(k) - \sum_{j=1}^{M_{\mathrm{TS}}} \beta_j(x_p(k))\overline{\theta}_j^T x(k)|\right\}\\ &\text{s.t.} \quad y_i(k) - \sum_{j=1}^{M_{\mathrm{TS}}} \beta_j(x_p(k))\overline{\theta}_j^T x(k) \le 0 \end{aligned} \tag{9}$$

where $y_i(k)$ denotes the ith measured data used in the model identification procedure. Let $t_1 := \max_i\{|y_i(k) - \sum_{j=1}^{M_{\mathrm{TS}}} \beta_j(x_p(k))\underline{\theta}_j^T x(k)|\}$ and $t_2 := \max_i\{|y_i(k) - \sum_{j=1}^{M_{\mathrm{TS}}} \beta_j(x_p(k))\overline{\theta}_j^T x(k)|\}$. From (8) and (9), $\underline{\theta}_j$ and $\overline{\theta}_j$ are obtained, respectively, as the solution to

$$\begin{aligned}&\min_{\underline{\theta}_j,\ t_1} \ t_1\\ &\text{s.t.} \quad y_i(k) - \sum_{j=1}^{M_{\mathrm{TS}}} \beta_j(x_p(k))\underline{\theta}_j^T x(k) \le t_1\\ &\qquad y_i(k) - \sum_{j=1}^{M_{\mathrm{TS}}} \beta_j(x_p(k))\underline{\theta}_j^T x(k) \ge 0 \qquad t_1 \ge 0 \end{aligned} \tag{10}$$

$$\begin{aligned}&\min_{\overline{\theta}_j,\ t_2} \ t_2\\ &\text{s.t.} \quad -y_i(k) + \sum_{j=1}^{M_{\mathrm{TS}}} \beta_j(x_p(k))\overline{\theta}_j^T x(k) \le t_2\\ &\qquad y_i(k) - \sum_{j=1}^{M_{\mathrm{TS}}} \beta_j(x_p(k))\overline{\theta}_j^T x(k) \le 0 \qquad t_2 \ge 0. \end{aligned} \tag{11}$$

From optimization problems (10) and (11), and since $f(z(k))$ is defined as $f(z(k)) = \sum_{j=1}^{M_{\mathrm{TS}}} \beta_j(x_p(k))\theta_j^T x(k)$, the upper and lower boundaries of $\hat{y}(k)$ are determined by $\overline{f}(z(k)) = \sum_{j=1}^{M_{\mathrm{TS}}} \beta_j(x_p(k))\overline{\theta}_j^T x(k)$ and $\underline{f}(z(k)) = \sum_{j=1}^{M_{\mathrm{TS}}} \beta_j(x_p(k))\underline{\theta}_j^T x(k)$, respectively. Since, with a certain confidence level, $\overline{f}(z(k))$ and $\underline{f}(z(k))$ define all possible realizations for $\hat{y}(k)$, the procedures as proposed in [31] can be used to generate scenarios with a reduced computational burden. Indeed, instead of exploring all the possible operating conditions, the pdf could be defined only within the interval defined by the INFUMO.

C. Interval Fuzzy Model-Based Robust Predictive Control Formulation

From (7), the predicted output of a system is given by

$$\hat{y}(k) = \sum_{j=1}^{M_{\mathrm{TS}}} \beta_j(x_p(k))\theta_j^T x(k)$$

where θ_j is a vector containing the parameters of the model associated with each rule. Then the fuzzy MPC is given by

$$\begin{aligned}&\min_{\tilde{u}(k)} \quad \sum_{l=1}^{N_p} J(y_{\mathrm{ref}}(k+l), \hat{y}(k+l), u(k+l-1))\\ &\text{s.t.} \quad \hat{y}(k+l) = \sum_{j=1}^{M_{\mathrm{TS}}} \beta_j(x_p(k+l))\theta_j^T x(k+l)\\ &\qquad u_{\min} \le u(k+l) \le u_{\max}\\ &\qquad \|u(k+l) - u(k+l-1)\| \le \Delta u_{\max}\\ &\qquad y_{\min} \le \hat{y}(k+l) \le y_{\max}. \end{aligned} \tag{12}$$

Often, linear consequences are used in the TS models. Indeed, consequences consisting of AutoRegressive models with eXogenous variable (ARX) are usual. Assume that the consequence of the jth rule of the TS model (7) has the form

$$\begin{aligned}&\hat{y}^j(k) + A_{q-1}^j\hat{y}^j(k-1) + \cdots + A_0^j\hat{y}^j(k-q)\\ &\quad = B_{q-1}^j u(k-1) + B_{q-2}^j u(k-2) + \cdots + B_0^j u(k-q). \end{aligned} \tag{13}$$

The corresponding controllable form of (13) is given by

$$\begin{aligned}\begin{bmatrix} x_1(k+1)\\ \vdots\\ x_q(k+1)\end{bmatrix} &= \underbrace{\begin{bmatrix} 0 & I & \cdots & 0\\ \vdots & 0 & \ddots & \vdots\\ 0 & \cdots & 0 & I\\ -A_0^j & -A_1^j & \cdots & -A_{q-1}^j\end{bmatrix}}_{A_{\mathrm{TS}}^j}\underbrace{\begin{bmatrix} x_1(k)\\ \vdots\\ x_q(k)\end{bmatrix}}_{\bar{x}(k)}\\ &\quad + \underbrace{\begin{bmatrix} 0\\ \vdots\\ 0\\ 1\end{bmatrix}}_{B_{\mathrm{TS}}^j} u(k)\\ \hat{y}^j(k) &= \underbrace{\begin{bmatrix} B_0^j & B_1^j & \cdots & B_{q-1}^j\end{bmatrix}}_{C_{\mathrm{TS}}^j}\begin{bmatrix} x_1(k)\\ \vdots\\ x_q(k)\end{bmatrix}. \end{aligned} \tag{14}$$

Let $\tilde{\hat{y}}^j(k)$ denote the predicted output given (14). Then

$$\begin{aligned}\underbrace{\begin{bmatrix} \hat{y}^j(k+1)\\ \vdots\\ \hat{y}^j(k+N_p)\end{bmatrix}}_{\tilde{\hat{y}}^j(k)} &= \underbrace{\begin{bmatrix} C_{\mathrm{TS}}^j A_{\mathrm{TS}}^j\\ \vdots\\ C_{\mathrm{TS}}^j\left(A_{\mathrm{TS}}^j\right)^{N_p}\end{bmatrix}}_{\Gamma^j}\bar{x}(k)\\ &\quad + \underbrace{\begin{bmatrix} C_{\mathrm{TS}}^j B_{\mathrm{TS}}^j & & \\ \vdots & \ddots & \\ C_{\mathrm{TS}}^j\left(A_{\mathrm{TS}}^j\right)^{N_p-1}B_{\mathrm{TS}}^j & \cdots & C_{\mathrm{TS}}^j B_{\mathrm{TS}}^j\end{bmatrix}}_{\Lambda^j}\underbrace{\begin{bmatrix} \hat{u}(k)\\ \vdots\\ \hat{u}(k+N_p-1)\end{bmatrix}}_{\tilde{u}(k)}. \end{aligned} \tag{15}$$

At time step k, assume $x_p(k)$ is equal to its measured value throughout N_p, then $\beta_j(x_p(k))$ is also constant. From (15), the predicted trajectory for $\tilde{\hat{y}}^j(k)$ can be

written as $\tilde{\hat{y}}^j(k) = \Gamma^j + \Lambda^j \tilde{u}(k)$. Since $\beta_j(x_p(k))$ is assumed constant, the predicted output of the system is given by $\tilde{\hat{y}}(k) = \sum_{j=1}^{M_{\text{TS}}} \beta_j(x_p(k))[\Gamma^j + \Lambda^j \tilde{u}(k)]$. Let $\Gamma = \sum_{j=1}^{M_{\text{TS}}} \beta_j(x_p(k))\Gamma^j$ and $\Lambda = \sum_{j=1}^{M_{\text{TS}}} \beta_j(x_p(k))\Lambda^j$. Then $\tilde{\hat{y}}(k) = \Gamma + \Lambda\tilde{u}(k)$.

Although the use of TS models into the MPC formulation provides a better approximation of nonlinear system dynamics, uncertainty still remains unmodeled. Since the uncertainty covers both the free and the forced system response $\tilde{\hat{y}}(k) = (\Gamma + \delta\Gamma) + (\Lambda + \delta\Lambda)\tilde{u}(k)$ (as in Section II-A). In this particular case, the INFUMO is used as a prediction model. Hence, $\overline{\theta} = \{\overline{\Gamma}, \overline{\Lambda}\}$ and $\underline{\theta} = \{\underline{\Gamma}, \underline{\Lambda}\}$, where $\overline{\Gamma}$ and $\underline{\Gamma}$, and $\overline{\Lambda}$ and $\underline{\Lambda}$ are the matrices associated with the free ($\overline{\Gamma}$ and $\underline{\Gamma}$) and forced ($\overline{\Lambda}$ and $\underline{\Lambda}$) responses of the INFUMO, respectively. Consequently, $\overline{f}(z(k)) = \sum_{j=1}^{M_{\text{TS}}} \beta_j(x_p(k))[\overline{\Gamma}^j + \overline{\Lambda}^j \tilde{u}(k)]$ and $\underline{f}(z(k)) = \sum_{j=1}^{M_{\text{TS}}} \beta_j(x_p(k))[\underline{\Gamma}^j + \underline{\Lambda}^j \tilde{u}(k)]$.

Let $\overline{\delta\Gamma}$, $\overline{\delta\Lambda}$, $\underline{\delta\Gamma}$, and $\underline{\delta\Lambda}$ be the uncertainties that generate the upper and lower boundaries of $\tilde{\hat{y}}(k)$. Then, $\overline{\Gamma} = \Gamma + \overline{\delta\Gamma}$, $\overline{\Lambda} = \Lambda + \overline{\delta\Lambda}$, $\underline{\Gamma} = \Gamma + \underline{\delta\Gamma}$, and $\underline{\Lambda} = \Lambda + \underline{\delta\Lambda}$. In this manner, $\Theta_\Gamma = \{\overline{\delta\Gamma}, \underline{\delta\Gamma}\}$, $\Theta_\Lambda = \{\overline{\delta\Lambda}, \underline{\delta\Lambda}\}$, $\mathbb{T} = \{(\overline{P}, \overline{q}, \overline{r}, \overline{\Gamma}, \overline{\Lambda}), (\underline{P}, \underline{q}, \underline{r}, \underline{\Gamma}, \underline{\Lambda})\}$, and $\mathbb{F} = \{(\overline{P}, \overline{q}, \overline{r}), (\underline{P}, \underline{q}, \underline{r})\}$. In accordance with the robust formulation presented in Section II-A, the associated worst case error $e_{\text{wc}}(\tilde{u}(k))$ of a candidate approximate solution $\tilde{u}(k)$ is given by

$$e_{\text{wc}}(\tilde{u}(k)) := \sup_{(P,q,r)} \{\tilde{u}^T(k) P \tilde{u}(k) + 2q\tilde{u}(k) + r \mid (P, q, r) \in \mathbf{conv}\{\mathbb{F}\}\}. \quad (16)$$

Thus, the fuzzy MPC (12) is reformulated in its robust programming form as (17). Note that in (17), the uncertainty of $\tilde{\hat{y}}(k)$ is explicitly included into the optimization problem. Moreover, such an optimization problem is convex and can be efficiently solved by numerical algorithms. In addition, it could be guaranteed that the solution converges to the global optimum

$$\begin{aligned} &\min_{\tilde{u}(k),t,f} \; t + f \\ &\text{s.t.} \quad \left\| P_i^{\frac{1}{2}} \tilde{u}(k) \right\|_2 \le t \\ &\qquad t + 2q_i\tilde{u}(k) + r_i \le f \\ &\qquad \begin{bmatrix} I \\ -I \\ \Delta_u \\ \Delta_u \\ \overline{\Lambda} \\ -\overline{\Lambda} \\ \underline{\Lambda} \\ -\underline{\Lambda} \end{bmatrix} \tilde{u}(k) \le \begin{bmatrix} \tilde{u}_{\max} \\ -\tilde{u}_{\min} \\ \tilde{\Delta u}_{\max} + \overline{u}(k-1) \\ \tilde{\Delta u}_{\max} - \overline{u}(k-1) \\ \tilde{y}_{\max} - \overline{\Gamma} \\ -\tilde{y}_{\min} + \overline{\Gamma} \\ \tilde{y}_{\max} - \underline{\Gamma} \\ -\tilde{y}_{\min} + \underline{\Gamma} \end{bmatrix}. \end{aligned} \quad (17)$$

It is important to remark that several methodologies can be used for generating the scenarios. In fact, the Monte Carlo simulation can be performed for generating several different situations within the interval provided by the INFUMO. Accordingly, several other scenarios could be included since a model is available to perform the predictions. In the next section, the formulation of the proposed robust predictive EMS is presented.

III. Proposed Scenario-Based Robust Energy Management System

A. Energy Management System

The proposed system is based on the EMS presented in [4]. The objectives of such an EMS are as follows:

1) to provide online power set-points for each generation units;
2) to adequately manage the water consumption;
3) to send the consumption signals to the customers according to the demand side management policies.

In this paper, the adequate management of the water consumption is not considered, thereby the proposed robust EMS is in charge of the following:

1) providing the power set-points for each generation unit;
2) sending the consumption signals to the customers according to the demand side management policies.

Nevertheless, the robust formulation can be easily adapted for including the signals for the water supply system. Unlike in [4], the proposed EMS uses the INFUMO for including the uncertainty of the NCES and the load in the optimization problem.

In the same way as in [4], the robust EMS minimizes the operational costs over a two-day horizon. At time step k, let $P_D(k)$, $P_B(k)$, and $S_L(k)$, respectively, denote the reference for the diesel and the battery bank and the demand signal for the customers. Let $P_S(k)$, $P_E(k)$, and $P_L(k)$, respectively, denote the predicted solar-based power, wind-based power, and demand. Let $C(k)$, $C_S(k)$, C_{NS}, and $C_H(k)$ denote the cost of diesel generation, the cost of starting up the diesel generator, the price of the unserved energy, and the cost of discharging the battery bank, respectively. Let T_s and $P_{\text{NS}}(k)$ denote the sample time and the unserved power, respectively. Then the EMS in [4] is formulated as

$$\begin{aligned} \min_{\substack{P_D(k+l),P_B(k+l),\\ P_{\text{Lo}}(k+l),S_L(k+l)}} \; & T_s \sum_{l=1}^{N_p} C(k+l) + \sum_{l=1}^{N_p} C_S(k+l) \\ & + C_{\text{NS}} T_s \sum_{l=1}^{N_p} P_{\text{NS}}(k+l) + C_H(N_p) \\ \text{s.t.} \quad & P_D(k+l) + P_I(k+l) + P_{\text{NS}}(k+l) \\ & = P_L(k+l) - P_{\text{Lo}}(k+l) - P_S(k+l) - P_E(k+l) \\ & V_D^{\min} \le V_D(k+l) \le V_D^{\max} \\ & E^{\min} \le E(k+l) \le E^{\max} \\ & S_L^{\min} \le S_L(k+l) \le S_L^{\max} \\ & P_D(k+l), \; P_{\text{NS}}(k+l) \ge 0 \\ & P_{\text{Lo}}(k+l) \le 0 \end{aligned} \quad (18)$$

where $P_I(k)$ and $P_{\text{Lo}}(k)$ are the powers provided by the inverter and the unused power, respectively; $V_D(k)$ and $E(k)$ are the volume of diesel and the energy of the battery bank, respectively; $V_D^{\min}$, $E^{\min}$, and $S_L^{\min}$ are the minimum

allowed values for the volume of diesel, for the energy of the battery bank, and for the customers' signal, repectively; and $V_D^{\max}$, $E^{\max}$, and $S_L^{\max}$ are the maximum allowed values for the volume of diesel, for the energy of the battery bank, and for the customers' signal, respectively. Note that $P_{\text{Lo}}(k)$ is a slack variable used to relax the power balance equality constraint. Physically, this variable indicates the energy to be dissipated for maintaining the balance in the microgrid.

With the purpose of solving the minimization problem (18), expressions that relate: 1) the costs $C(k)$ and $C_S(k)$; 2) the powers $P_I(k)$ and $P_{\text{NS}}(k)$; 3) the volume $V_D(k)$; and 4) the available energy on the battery bank $E(k)$, with the decision variables $P_D(k)$, $P_B(k)$, $S_L(k)$, and $P_{\text{Lo}}(k)$ being required. Therefore, prediction models for $P_I(k)$, $q_D(k)$, $V_D(k)$, and $E(k)$ must be derived.

From [4], the cost associated with the diesel generation is proportional to the amount of diesel used, i.e., $C(k) = C_D q_D(k)$, with C_D and $q_D(k)$ being the average diesel price and the diesel fuel consumption, respectively. Moreover, P_D and $q_D(k)$ are related by a nonlinear nonconvex function. Such a relationship is approximated by a set of piecewise linear functions. Let $B_D(P_D(k))$ denote the weighting function that defines the contribution of each piecewise linear model, and θ_D and θ_{PD} be the matrices containing the intercept and the slope of each linear model. Then the relation between P_D and $q_D(k)$ is expressed as

$$q_D(k) = B_D(P_D(k))\,(\theta_D + \theta_{\text{PD}} P_D(k)). \tag{19}$$

As in Section II, assume $B_D(P_D(k))$ to be constant over N_p. Using (19), the diesel consumption throughout the prediction horizon is given by

$$\underbrace{\begin{bmatrix} q_D(k+1) \\ \vdots \\ q_D(k+N_p) \end{bmatrix}}_{\tilde{q}_D(k)} = \underbrace{\begin{bmatrix} B_D(P_D(k)) & & \\ & \ddots & \\ & & B_D(P_D(k)) \end{bmatrix}}_{\tilde{B}(P_D(k))} \times \left(\underbrace{\begin{bmatrix} \theta_D \\ \vdots \\ \theta_D \end{bmatrix}}_{\Gamma_{qD}} + \underbrace{\begin{bmatrix} \theta_{\text{PD}} & & \\ & \ddots & \\ & & \theta_{\text{PD}} \end{bmatrix}}_{\Lambda_{qD}} \underbrace{\begin{bmatrix} P_D(k+1) \\ \vdots \\ P_D(k+N_p) \end{bmatrix}}_{\tilde{P}_D(k)} \right).$$

The evolution of the diesel consumption is linked to $V_D(k)$. In fact, the amount of diesel cannot exceed the maximum and minimum values of $V_D(k)$. As aforementioned, at time step k, let $V_D(k)$ be the measured volume of diesel. Then, its variations can be estimated as the difference between the measured volume and the amount of diesel used in the generation process. Mathematically, this is formulated as

$$V_D(k+1) = V_D(k) - q_D(k+1).$$

Let $\tilde{V}_D(k) = [V_D(k+1), \ldots, V_D(k+N_p)]^T$ be the predicted trajectory of the diesel volume throughout N_p. Substituting expression (19) for $q_D(k)$, the resulting expression for predicting the trajectory of $V_D(k)$ becomes

$$\begin{bmatrix} V_D(k+1) \\ \vdots \\ V_D(k+N_p) \end{bmatrix} = \underbrace{I V_D(k) - \begin{bmatrix} B_D(P_D(k))\theta_D \\ \vdots \\ N_p B_D(P_D(k))\theta_D \end{bmatrix}}_{\Gamma_{\text{VD}}} - \underbrace{\begin{bmatrix} B_D(P_D(k))\theta_{\text{PD}} & & \\ \vdots & \ddots & \\ B_D(P_D(k))\theta_D & \ldots & B_D(P_D(k))\theta_D \end{bmatrix}}_{\Lambda_{\text{VD}}} \begin{bmatrix} P_D(k+1) \\ \vdots \\ P_D(k+N_p) \end{bmatrix}$$

with I an identity matrix, $I \in \mathbb{R}^{N_p \times N_p}$. The prediction model for computing $\tilde{V}_D(k)$ is the following:

$$\tilde{V}_D(k) = \Gamma_{\text{VD}} + \Lambda_{\text{VD}} \tilde{P}_D(k). \tag{20}$$

In the case of the battery bank, the power provided by the inverter $P_I(k)$ is determined by the charging and discharging features of the battery. Let P_{lo} denote the internal power consumed by the inverter. Let η_d and η_c denote the inverter losses in both operation modes, namely, discharge and charge modes, respectively. Assume that $P_B(k) \geq 0$ if the battery bank is being discharged and that $P_B(k) < 0$ if the battery is being charged. Then the power provided by the inverter is given by [4]

$$P_I(k) = \begin{cases} \eta_d P_B(k) - P_{\text{lo}}, & P_B(k) \geq 0 \\ \dfrac{P_B(k)}{\eta_c} - P_{\text{lo}}, & P_B(k) < 0. \end{cases} \tag{21}$$

Expression (21) has a discontinuity in $P_B(k) = 0$. Such a discontinuity may affect the solution of the minimization problem (18). Thus, an approximated model for $P_I(k)$ is proposed. Let $P_B^+(k)$ and $P_B^-(k)$ be auxiliary variables such that $P_B^+(k) \geq 0$, $P_B^-(k) \leq 0$, and $P_B^+(k)P_B^-(k) = 0$. Then (21) can be rewritten as

$$P_I(k) = \eta_d P_B^+(k) + \frac{P_B^-(k)}{\eta_c} - P_{\text{lo}}. \tag{22}$$

In (22), the constraint $P_B^+(k)P_B^-(k) = 0$ prevents charging and discharging the battery at the same time. Let $\tilde{P}_I(k) = [P_I(k+1), \ldots, P_I(k+N_p)]^T$ and $\Gamma_I = [-P_{\text{lo}}, \ldots, -P_{\text{lo}}]^T \in \mathbb{R}^{N_p}$, and Λ_I^+, and Λ_{I}^- be the diagonal matrices whose elements are η_d and $1/\eta_c$, respectively. Then the predicted trajectory of the power provided by the inverter is given by

$$\tilde{P}_I(k) = \Gamma_I + \Lambda_I^+ \tilde{P}_B^+(k) + \Lambda_I^- \tilde{P}_B^-(k)$$

with $\tilde{P}_B^+(k) = [P_B^+(k+1), \ldots, P_B^+(k+N_p)]^T$ and $\tilde{P}_B^-(k) = [P_B^-(k+1), \ldots, P_B^-(k+N_p)]^T$.

With the addition of $P_B^+(k)$ and $P_B^-(k)$, two more constraints arise, namely, $0 \leq P_B^+(k) \leq P_B^{\max}$ and $P_B^{\min}(k) \leq P_B^-(k) \leq 0$. These constraints are related with the maximum power the battery is able to provide and with the maximum power the battery demands in the charging process. In the first case, the maximum power is limited by the current constraints of the inverter. But in the second case, the power demanded by the battery is a function of the state of charge (SoC). Such a dependency obeys a nonlinear relationship [4]. However, in this paper, piecewise linear functions are used to make

an approximation. Let $E(k)$ denote the available energy in the battery bank. Then

$$P_B^{\min}(k) = B_B(E(k))\,(\theta_E + \theta_{\text{PB}} E(k))\,.$$

Let η_B denote the efficiency of the battery bank. Then an energy balance yields

$$\begin{aligned} E(k+1) = {} & E(k) - T_s \eta_B^+ P_B^+(k+1) \\ & - T_s \eta_B^- P_B^-(k+1) + T_s \eta_B P_{\text{lo}} \end{aligned} \tag{23}$$

where $\eta_B^+ = \eta_B \eta_d$ and $\eta_B^- = (\eta_B/\eta_c)$ are the efficiency coefficients of the battery bank in the charging and discharging processes, respectively. Let $\tilde{E}(k) = [E(k+1), \ldots, E(k+N_p)]^T$ and $\Gamma_E = IE(k) - T_s \Gamma_I$. Then the estimated energy over N_p is determined by

$$\tilde{E}(k) = \Gamma_E - T_s \Lambda_I^+ \tilde{P}_B^+(k) - T_s \Lambda_I^- \tilde{P}_B^-(k).$$

Based on the predicted available energy $\tilde{E}(k)$, the expected maximum power demanded by the battery in the charging process is computed as

$$\tilde{P}_B^{\min}(k) = \Gamma_B + T_s \Lambda_B^+ \tilde{P}_B^+(k) + T_s \Lambda_B^- \tilde{P}_B^-(k) \tag{24}$$

where $\tilde{P}_B^{-\min}(k) = [P_B^{-\min}(k+1), \ldots, P_B^{-\min}(k+N_p)]$, and

$$\Gamma_B = \begin{bmatrix} B_B(E(k)) & & \\ & \ddots & \\ & & B_B(E(k)) \end{bmatrix} \times \left(\begin{bmatrix} \theta_E \\ \vdots \\ \theta_E \end{bmatrix} + \begin{bmatrix} \theta_{\text{PB}} & & \\ & \ddots & \\ & & \theta_{\text{PB}} \end{bmatrix} \Gamma_E \right)$$

$$\Lambda_B^+ = - \begin{bmatrix} B_B(E(k)) & & \\ & \ddots & \\ & & B_B(E(k)) \end{bmatrix} \begin{bmatrix} \theta_{\text{PB}} & & \\ & \ddots & \\ & & \theta_{\text{PB}} \end{bmatrix} \Lambda_I^+$$

$$\Lambda_B^- = - \begin{bmatrix} B_B(E(k)) & & \\ & \ddots & \\ & & B_B(E(k)) \end{bmatrix} \begin{bmatrix} \theta_{\text{PB}} & & \\ & \ddots & \\ & & \theta_{\text{PB}} \end{bmatrix} \Lambda_I^-.$$

Thus, the inequality $P_B^{\min}(k) \le P_B^-(k) \le 0$ becomes $(T_s \Lambda_B^- - I)\tilde{P}_B^-(k) + T_s \Lambda_B^+ \tilde{P}_B^+(k) \le -\Gamma_B$ and $\tilde{P}_B^-(k) \le 0$.

With the models previously derived, the optimization problem (18) becomes (25), shown at the bottom of the page. In (25), vectors $\tilde{V}_D^{\max}$, $\tilde{V}_D^{\min}$, $\tilde{E}^{\max}$, $\tilde{E}^{\min}$, and $\tilde{P}_B^{\max} \in \mathbb{R}^{N_p}$ denote the maximum and minimum values of their respective variables. Furthermore, the operation $\tilde{P}_B^+(k) \cdot \tilde{P}_B^-(k)$ indicates the component to component product.

Note that computing the solution of (25) requires the values of $\tilde{P}_S(k) = [P_S(k+1), \ldots, P_S(k+N_p)]^T$, $\tilde{P}_E(k) = [P_E(k+1), \ldots, P_E(k+N_p)]^T$, and $\tilde{P}_L(k) = [P_L(k+1), \ldots, P_L(k+N_p)]^T$. These values are needed for the power balance constraint. In the next section, how to obtain these values is addressed, taking into account their inherent uncertainty.

B. Prediction Models for Renewable Energy Sources and Load Forecasting

A relationship between the different variables involved into the optimization problem (25) is derived in Section III-A. But in such a relationship, deriving a function that relates the unserved power $\tilde{P}_{\text{NS}}(k)$ with the decision variables in (25) is still needed. From (25)

$$\tilde{P}_{\text{NS}}(k) = \tilde{P}_L(k) - \tilde{P}_{\text{Lo}}(k) - \tilde{P}_S(k) - \tilde{P}_E(k) - \tilde{P}_D(k) - \tilde{P}_I(k).$$

Then, the prediction of the unserved energy is closely related with the available energy in the NCES and the load forecasting. Therefore, the expressions for computing $\tilde{P}_S(k)$, $\tilde{P}_E(k)$, and $\tilde{P}_L(k)$ should be found. In general, $\tilde{P}_S(k)$ and $\tilde{P}_E(k)$ depend on the accuracy of the weather forecasting models (among others wind speed and direction, solar radiation, and temperature), while $\tilde{P}_L(k)$ depends upon the consumption patterns of the customers.

In [32]–[34], several weather forecasting models have been reported. These models cover both numerical and empirical

$$\begin{aligned} \min_{\substack{\tilde{P}_D(k), \tilde{P}_B^+(k), \\ \tilde{P}_B^-(k), \tilde{P}_{\text{Lo}}(k), \tilde{S}_L(k)}} \quad & \bar{I}^T \left(T_s \tilde{C}(k) + \tilde{C}_S(k) + C_{\text{NS}} T_s \tilde{P}_{\text{NS}}(k) \right) + C_H(N_p) \\ \text{s.t.} \quad & \tilde{P}_{\text{NS}}(k) = \tilde{P}_L(k) - \tilde{P}_{\text{Lo}}(k) - \tilde{P}_S(k) - \tilde{P}_E(k) - \tilde{P}_D(k) - \tilde{P}_I(k) && \text{Power balance} \\ & \tilde{P}_I(k) = \Gamma_I + \Lambda_I^+ \tilde{P}_B^+(k) + \Lambda_I^- \tilde{P}_B^-(k) && \text{Inverter power} \\ & \tilde{q}_D(k) = \tilde{B}(P_D(k)) \left(\Gamma_{qD} + \Lambda_{qD}^+ \tilde{P}_D(k) \right) && \text{Diesel consumption} \\ & \left. \begin{array}{l} \Lambda_{\text{VD}} \tilde{P}_D(k) \le \tilde{V}_D^{\max} - \Gamma_{\text{VD}} \\ -\Lambda_{\text{VD}} \tilde{P}_D(k) \le \Gamma_{\text{VD}} - \tilde{V}_D^{\min} \end{array} \right\} && \text{Diesel storage constraints} \\ & \left. \begin{array}{l} -T_s \Lambda_I^+ \tilde{P}_B^+(k) - T_s \Lambda_I^- \tilde{P}_B^-(k) \le \tilde{E}^{\max} - \Gamma_E \\ T_s \Lambda_I^+ \tilde{P}_B^+(k) + T_s \Lambda_I^- \tilde{P}_B^-(k) \le \Gamma_E - \tilde{E}^{\min} \\ (T_s \Lambda_B^- - I) \tilde{P}_B^-(k) + T_s \Lambda_B^+ \tilde{P}_B^+(k) \le -\Gamma_B \\ \tilde{P}_B^+(k) \le \tilde{P}_B^{\max} \\ \tilde{P}_B^+(k) \cdot \tilde{P}_B^-(k) = 0 \end{array} \right\} && \text{Battery constraints} \\ & \left. \begin{array}{l} \tilde{S}_L(k) \le \tilde{S}_L^{\max}, \quad -\tilde{S}_L(k) \le -S_L^{\min} \\ P_D(k+l), \ P_{\text{NS}}(k+l), \quad \tilde{P}_B^+(k) \ge 0 \\ P_{\text{Lo}}(k+l), \quad \tilde{P}_B^-(k) \le 0 \end{array} \right\} && \text{Operating constraints} \end{aligned} \tag{25}$$

prediction models. Once weather conditions are predicted, they must be transformed into available energy. For estimating the demand, correlations are made for adapting parameters of autoregressive models according to the season and predicted weather conditions. But, notwithstanding the amount of approaches reported in the literature, uncertainty in NCES and load forecasting remains as an open issue. This motivates the use of the INFUMO rather than identifying exact demand and NCES models. The INFUMO allows taking into account both the dynamic behavior and the uncertainty present in NCES and load forecasting processes. In the literature, several confidence interval modeling approaches have been proposed. Mainly, they are based on multimodel representation of the system [26]–[29]. In this paper, the methodology described in Section II-B is considered.

At time step k, let $x_{pS}(k), x_{pE}(k)$, and $x_{pL}(k)$ denote the premise variables of the fuzzy models representing the solar power, the wind power, and the load, respectively. For these, let x_S, x_E, and x_L denote the variables of the consequences, $\beta_{Sj}(x_{pS}(k))$, $\beta_{Ej}(x_{pE}(k))$, and $\beta_{Lj}(x_{pL}(k))$ be the normalized membership function, and $\theta_S j$, $\theta_E j$, and $\theta_L j$ denote the parameters of the linear model associated with the jth rule. Then the prediction models for the available solar power, wind power, and demand are given by the following expressions:

$$P_S(k) = \sum_{j=1}^{M_S} \beta_{Sj}(x_{pS}(k))\theta_{sj}^T x_S(k) \tag{26}$$

$$P_E(k) = \sum_{j=1}^{M_E} \beta_{Ej}(x_{pE}(k))\theta_{Ej}^T x_E(k) \tag{27}$$

$$P_L(k) = \sum_{j=1}^{M_L} \beta_{Lj}(x_{pL}(k))\theta_{Lj}^T x_L(k). \tag{28}$$

Based on expressions (26)–(28) and on the procedure introduced in Section II-A, a set of parameters $\overline{\theta}_S j, \overline{\theta}_E j, \overline{\theta}_L j$ and $\underline{\theta}_S j, \underline{\theta}_E j, \underline{\theta}_L j$ are obtained in such a way that the trajectories of $P_S(k)$, $P_E(k)$, and $P_L(k)$ are bounded above and below with a certain confidence level.

With regard to the modeling of the NCES, let $B_S(x_{pS}(k)) = [\beta_{s1}(x_{pS}(k)), \ldots, \beta_{sM_S}(x_{pS}(k))]$ and also let $B_E(x_{pE}(k)) = [\beta_{E1}(x_{pE}(k)), \ldots, \beta_{EM_E}(x_{pE}(k))]$. Besides, assume that $B_S(x_{pS}(k))$ and $B_{pE}(x_{pE}(k))$ are constant throughout N_p. Then the predicted output of each rule in the fuzzy models (26) and (27) can be written as (15). As a consequence, the prediction models for the solar and wind-based energy sources are (respectively) as follows: $\tilde{P}_S(k) = \Gamma_{pS} + \Lambda_{pS}\tilde{R}(k)$ and $\tilde{P}_E(k) = \Gamma_{pE} + \Lambda_{pE}\tilde{v}(k)$. In this case, $\Gamma_{pS} = \sum_{j=1}^{M_S} \beta_{Sj}(x_{pS}(k))\Gamma_S^j$, $\Gamma_{pE} = \sum_{j=1}^{M_E} \beta_{Ej}(x_{pE}(k))\Gamma_E^j$, $\Lambda_{pS} = \sum_{j=1}^{M_S} \beta_{Sj}(x_{pS}(k))\Lambda_S^j$, and $\Lambda_{pE} = \sum_{j=1}^{M_E} \beta_{Ej}(x_{pE}(k))\Lambda_E^j$, and $\tilde{R}(k)$ and $\tilde{v}(k)$ being the radiation and the wind speed sequences over the prediction horizon. In this paper, it is assumed that a data base with the values of radiation and the wind speed is available.

Due to $\Gamma_S, \Gamma_{pE}, \Lambda_S$, and Λ_{pE}, respectively, depend only on θ_S and θ_E, the upper and lower boundaries are computed as a function of $\overline{\theta}_S$ and $\overline{\theta}_E$, and $\underline{\theta}_S$ and $\underline{\theta}_E$, with θ_S and θ_E being the matrices whose elements are the parameters of the solar-based and wind-based fuzzy models (26) and (27), respectively. Let $\overline{\tilde{P}}_S(k)$, $\overline{\tilde{P}}_E(k)$, $\underline{\tilde{P}}_S(k)$, and $\underline{\tilde{P}}_E(k)$ be the upper and lower boundaries for $\tilde{P}_S(k)$ and $\tilde{P}_E(k)$, respectively. Then according to the corresponding INFUMO $\overline{\tilde{P}}_S(k)$, $\overline{\tilde{P}}_E(k)$, $\underline{\tilde{P}}_S(k)$, and $\underline{\tilde{P}}_E(k)$ have the form (29)–(32). In these expressions, $\overline{\Gamma}_S, \overline{\Lambda}_S, \underline{\Gamma}_S$, and $\underline{\Lambda}_S$ are obtained from $\overline{\theta}_S$ and $\underline{\theta}_S$, respectively, while $\overline{\Gamma}_E, \overline{\Lambda}_E, \underline{\Gamma}_E$, and $\underline{\Lambda}_E$ are, respectively, obtained from $\overline{\theta}_E$ and $\underline{\theta}_E$

$$\overline{\tilde{P}}_S(k) = \overline{\Gamma}_S + \overline{\Lambda}_S\tilde{R}(k) \tag{29}$$

$$\overline{\tilde{P}}_E(k) = \overline{\Gamma}_E + \overline{\Lambda}_E\tilde{v}(k) \tag{30}$$

$$\underline{\tilde{P}}_S(k) = \underline{\Gamma}_S + \underline{\Lambda}_S\tilde{R}(k) \tag{31}$$

$$\underline{\tilde{P}}_E(k) = \underline{\Gamma}_E + \underline{\Lambda}_E\tilde{v}(k). \tag{32}$$

With regard to the load forecasting model, let $B_L(x_{pL}(k)) = [\beta_{L1}(x_{pL}(k)), \ldots, \beta_{LM_L}(x_{pL}(k))]$. As in the case of the NCES, assume that $B_L(x_{pL}(k))$ is constant throughout N_p. Then the predicted output of each rule of the load forecasting model (28) has the form (15). Consequently, the predicted demand is given by $\tilde{P}_L(k) = \Gamma_{pL} + \Lambda_{pL}\tilde{T}(k)$, where $\Gamma_{pL} = \sum_{j=1}^{M_L} \beta_{Lj}(x_{pL}(k))\Gamma_L^j$, $\Lambda_{pL} = \sum_{j=1}^{M_L} \beta_{Lj}(x_{pL}(k))\Lambda_L^j$, and $\tilde{T}(k)$ is the temperature over the prediction horizon. Just as in the case of the NCES, Γ_{pL} and Λ_{pL} depend only on θ_L, a matrix whose elements are the parameters of the fuzzy model (28). Then the upper and lower boundaries for $\tilde{P}_L(k)$ are computed based on $\overline{\theta}_L$ and $\underline{\theta}_L$. Let $\overline{\tilde{P}}_L(k)$ and $\underline{\tilde{P}}_L(k)$ denote the upper and lower boundaries for $\tilde{P}_L(k)$, respectively. Then in accordance with the INFUMO, $\overline{\tilde{P}}_L(k)$ and $\underline{\tilde{P}}_L(k)$ have the form

$$\overline{\tilde{P}}_L(k) = \overline{\Gamma}_{pL} + \overline{\Lambda}_{pL}\tilde{T}(k) \tag{33}$$

$$\underline{\tilde{P}}_L(k) = \underline{\Gamma}_{pL} + \underline{\Lambda}_{pL}\tilde{T}(k). \tag{34}$$

Since in [4] the demand is defined as the product $\tilde{P}_L(k) \cdot \tilde{S}_L(k)$, with abuse of notation, let redefine $\tilde{P}_L(k) = (\Gamma_{pL} + \Lambda_{pL}\tilde{T}(k)) \cdot \tilde{S}_L(k)$, with the product $x \cdot y$ indicating the element to element product. Note that $\tilde{P}_L(k)$ depends only on the estimated demand and the expected load shifting $\tilde{S}_L(k)$. Thence, it is possible to assume that $\tilde{P}_L(k)$ only has a forced response, that is, $\tilde{P}_L(k) = \Lambda_L\tilde{S}_L(k)$, where Λ_L is a diagonal matrix whose elements are given by the fuzzy model $\Gamma_{pL} + \Lambda_{pL}\tilde{T}(k)$. Thus, from (33) and (34), the upper and lower boundaries for the demand (including the load shifting action) are given by

$$\overline{\tilde{P}}_L(k) = \overline{\Lambda}_L\tilde{S}_L(k) \tag{35}$$

$$\underline{\tilde{P}}_L(k) = \underline{\Lambda}_L\tilde{S}_L(k) \tag{36}$$

with $\tilde{S}_L(k) \in \mathbb{R}^{N_p}$ the sequence of load shifting factors over the prediction horizon, and $\overline{\Lambda}_L$ and $\underline{\Lambda}_L$ the values of Λ_L computed with $\overline{\theta}_L$ and $\underline{\theta}_L$, respectively. In the next section, the proposed robust EMS is described.

C. Robust Energy Management System

Prediction models for the conventional energy sources, for the NCES, and for the load were derived

in Sections III-A and III-B. In these models, the predicted behavior was related to the decision variables of the minimization problem (18). Regarding the minimization problem (18), these prediction models were also used to express the constraints as functions of the decision variables. Consequently, the minimization problem (25) was obtained. Let $\widetilde{u}(k) = [\tilde{P}_D^T(k), \tilde{P}_B^{+T}(k), \tilde{P}_B^{-T}(k), \tilde{P}_{\text{Lo}}^T(k), \tilde{S}_L^T(k)]^T$. With the models derived in Sections III-A and III-B for $\tilde{P}_I(k)$, $\tilde{P}_L(k)$, $\tilde{P}_S(k)$, and $\tilde{P}_E(k)$, the power balance constraint in (25) becomes

$$\tilde{P}_{\text{NS}}(k) = \underbrace{-\left(\Gamma_S + \Gamma_E + \Gamma_I + \Lambda_S \tilde{R}_S(k) + \Lambda_E \tilde{v}_E(k)\right)}_{\Gamma_{\text{NS}}} + \underbrace{\left[I \ -\Lambda_I^+ \ -\Lambda_I^- \ -I \ \Lambda_L\right]}_{\Lambda_{\text{NS}}} \widetilde{u}(k). \tag{37}$$

In (37), the terms $\Lambda_S \tilde{R}_S(k) + \Lambda_E \tilde{v}_E(k)$ and Λ_L are uncertain. Accordingly, the uncertainty in the prediction of the unserved power $\tilde{P}_{\text{NS}}(k)$ covers both its free and its forced response. Thus, $\tilde{P}_{\text{NS}}(k) = (\Gamma_{\text{NS}} + \delta\Gamma_{\text{NS}}) + (\Lambda_{\text{NS}} + \delta\Lambda_{\text{NS}})\,\widetilde{u}(k)$.

Let $\tilde{P}_D(k) = C_1\widetilde{u}(k)$, $\tilde{P}_B^+(k) = C_2\widetilde{u}(k)$, $\tilde{P}_B^-(k) = C_3\widetilde{u}(k)$, $\tilde{P}_{\text{Lo}}^T(k) = C_4\widetilde{u}(k)$, and $\tilde{S}_L(k) = C_5\widetilde{u}(k)$, with C_1–C_5 selection matrices with the adequate dimension. Since $C(k+l) = C_D q(k+l)$, the diesel generation over the prediction horizon turns into $\tilde{C}(k) = C_D\Gamma_q + C_D\Lambda_q C_1\widetilde{u}(k)$, with $\Gamma_q = \tilde{B}(P_D(k))\Gamma_{qD}$ and $\Lambda_q = \tilde{B}(P_D(k))\Lambda_{qD}$. For $C_S(k)$, in [4], an approach based on binary variables was suggested. However, such an approach required the estimation of the SoC and of the state of health of the battery bank, which is an open issue in the specialized literature. For addressing this drawback, in this paper, an alternative formulation is proposed. Let λ denote the fixed cost for changing the operating mode of the diesel generator. Then $C_S(k)$ is defined as $C_S(k) := \lambda\Delta P_D(k)$, with $\Delta P_D(k) = P_D(k) - P_D(k-1)$. Let $P_{\text{Do}} = [-P_D(k), 0, \ldots, 0]^T$ and Δ_{PD} be defined as

$$\Delta_{\text{PD}} = \begin{bmatrix} I & & & \\ -I & I & & \\ & \ddots & \ddots & \\ & & -I & I \end{bmatrix} C_1.$$

Then $C_S(k)$ is computed in terms of the decision variables $\widetilde{u}(k)$ as $C_S(k) = \Delta_{\text{PD}}\widetilde{u}(k) + P_{\text{Do}}$. With this definition, the following conditions hold: 1) If $\Delta\tilde{P}_D(k) > 0$, the value of the cost function increases. 2) If $\Delta\tilde{P}_D(k) = 0$, the value of the cost function remains constant. 3) If $\Delta\tilde{P}_D(k) < 0$, the value of the cost function decreases. With these considerations, once the diesel generator is started, it is expected that the EMS tends to maintain the same operating conditions or tends to turn it OFF.

Finally, recall that $C_H(N_p)$ denotes the cost of using the battery bank. An expression for $C_H(N_p)$ based on the estimation of the SoC is proposed in [4]. Due to the aforementioned issues with respect to the estimation of the SoC, in this paper, an alternative formulation for $C_H(N_p)$ is proposed. At time step k, let $C_H(k)$ denote the cost of using the battery bank. Let E_f represent its maximum desired discharge level. Also, let F_t denote the investment cost due to the degradation of the battery bank. Then $C_H(k)$ is defined as $C_H(k) := F_t(E_f - E(k))$. With this formulation, it is expected that the EMS maintains the energy of the battery bank over E_f. Indeed, the value of the cost function increases if $E(k) < E_f$. By contrast, with the formulation in [4], the proposed definition of $C_H(k)$ penalizes the battery use throughout N_p. Therefore, a better use of this energy resource is also expected. Let $\tilde{C}_H(k) = [C_H(k+1), \ldots, C_H(k+N_p)]^T$. Then, $\tilde{C}_H(k) = \Gamma_H + \Lambda_H\widetilde{u}(k)$, with $\Gamma_H = F_r(\tilde{E}_f - \Gamma_E)$ and $\Lambda_H = F_t(\Lambda_I^+ C_2 + \Lambda_I^- C_3)$.

Let $G_i \in \mathbb{R}^{N_p \times N_p}$, $i = 1, \ldots, N_p$, be the diagonal matrices with their ith element of the diagonal equals to one and the remaining elements equals to zero. Then the equality constraint $\tilde{P}_B^+(k) \cdot \tilde{P}_B^-(k) = 0$ can be equivalently written as the set of quadratic constraints $\widetilde{u}^T(k)C_2^T G_i C_3\widetilde{u}(k) = 0$, $i = 1, \ldots, N_p$. Let $t \in \mathbb{R}$ be an auxiliary variable. Using the Cauchy–Schwarz inequality, the equality constraint $\widetilde{u}^T(k)\bar{G}_i^{(1/2)}\widetilde{u}(k) = 0$, $i = 1, \ldots, N_p$, is reformulated as $\|\bar{G}_i\widetilde{u}(k)\|_2 \leq t$. The formulation of the constraint $\tilde{P}_B^+(k) \cdot \tilde{P}_B^-(k) = 0$ as the norm constraint $\|\bar{G}_i\widetilde{u}(k)\|_2 \leq t$ allows formulating (25) as an SOCP problem. From the prediction models derived for the conventional energy sources, and from the INFUMO deduced for the NCES and the demand, the parameters q and r in (3) are given by

$$q = \bar{I}^T\left(T_s C_D\Lambda_q C_1 + \Delta_{\text{PD}} + T_s C_{\text{NS}}(\Lambda_{\text{NS}} + \delta\Lambda_{\text{NS}}) + \Lambda_H\right)$$
$$r = \bar{I}^T\left(T_s C_D\Gamma_q + P_{\text{Do}} + T_s C_{\text{NS}}(\Gamma_{\text{NS}} + \delta\Gamma_{\text{NS}}) + \Gamma_H\right).$$

Then, the cost function in (25) becomes $J(\widetilde{u}(k)) = q\widetilde{u}(k) + r + t$. Hence, using the INFUMO to define the uncertain set, and relating this set with both q and r, the EMS problem (25) can be equivalently written as (17).

Based on the their definitions, q is function of $\delta\Lambda_{\text{NS}}$ and r is function of $\delta\Gamma_{\text{NS}}$. Therefore, $q = \bar{q} + \delta q$ and $r = \bar{r} + \delta r$, where $\bar{q} = \bar{I}^T(T_s C_D\Lambda_q C_1 + \Delta_{\text{PD}} + T_s C_{\text{NS}}\Lambda_{\text{NS}} + \Lambda_H)$, $\bar{r} = \bar{I}^T(T_s C_D\Gamma_q + P_{\text{Do}} + T_s C_{\text{NS}}\Gamma_{\text{NS}} + \Gamma_H)$, $\delta q = \bar{I}^T T_s C_{\text{NS}}\delta\Lambda_{\text{NS}}$, and $\delta r = \bar{I}^T T_s C_{\text{NS}}\delta\Gamma_{\text{NS}}$, thereby there is a mapping from the model to the uncertainty in the parameters of $J(\widetilde{u}(k))$. Specifically, associated with each pair $(\delta\Gamma_{\text{NS}}, \delta\Lambda_{\text{NS}})$, there is a pair $(\delta q, \delta r)$ and therefore a pair (q, r). Let $\Theta_\Gamma = \{\delta\Gamma_{\text{NS}1}, \ldots, \delta\Gamma_{\text{NS}M}\}$ and $\Theta_\Lambda = \{\delta\Lambda_{\text{NS}1}, \ldots, \delta\Lambda_{\text{NS}M}\}$. Then, the set of tuples

$$\mathbb{T} = \{(q_1, r_1, \delta\Gamma_{\text{NS}1}, \delta\Lambda_{\text{NS}1}), \ldots, (q_M, r_M, \delta\Gamma_{\text{NS}M}, \delta\Lambda_{\text{NS}M})\}$$

defines all the possible scenarios arising from Θ_Γ and Θ_Λ. In the proposed EMS, the total amount of scenarios is eight. The scenarios arise from the combination of the upper and lower boundary predictions provided by the INFUMO. These scenarios are summarized in Table I.

Let $\mathbb{F} = \{(q_1, r_1), \ldots, (q_M, r_M)\}$. Then the worst case error $e_{\text{wc}}(\widetilde{u}(k))$ of a candidate approximate solution $\widetilde{u}(k)$ is given by

$$e_{\text{wc}}(\widetilde{u}(k)) = \sup_{q,r,\Gamma_{\text{NS}},\Lambda_{\text{NS}}} \{q\widetilde{u}(k) + r \mid (q, r) \in \textbf{conv}\{\mathbb{F}\}\}. \tag{38}$$

TABLE I
SCENARIOS GENERATED WITH THE INFUMO FOR PREDICTING THE AVAILABLE ENERGY IN THE NCES AND FOR THE LOAD FORECASTING

	$\tilde{P}_{\mathrm{L}}(k)$	$\tilde{P}_{\mathrm{S}}(k)$	$\tilde{P}_{\mathrm{E}}(k)$
Scenario (m):			
1	Upper	Upper	Upper
2	Upper	Upper	Lower
3	Upper	Lower	Upper
4	Upper	Lower	Lower
5	Lower	Upper	Upper
6	Lower	Upper	Lower
7	Lower	Lower	Upper
8	Lower	Lower	Lower

Hence, the robust EMS based on scenarios is given by the SOCP problem

$$\begin{aligned}
&\min_{\widetilde{u}(k),t,d} \quad t+d \\
&\text{s.t.} \quad r_m + q_m\widetilde{u}(k) \le d, \quad m=1,\ldots,8 \\
&\quad \left\|\bar{G}_i^{\frac{1}{2}}\widetilde{u}(k)\right\|_2 \le t, \quad i=1,\ldots,N_p \\
&\quad \begin{bmatrix} \Lambda_{\mathrm{VD}}C_1 \\ -\Lambda_{\mathrm{VD}}C_1 \\ -T_s\Lambda_I^+C_2 - T_s\Lambda_I^-C_3 \\ T_s\Lambda_I^+C_2 + T_s\Lambda_I^-C_3 \\ (T_s\Lambda_B^- - I)C_3 + T_s\Lambda_B^+C_2 \\ -\Lambda_{\mathrm{NS}m} \\ C_2 \\ C_5 \\ -C_5 \\ -C_1 \\ -C_2 \\ C_4 \\ C_3 \end{bmatrix} \widetilde{u}(k) \le \begin{bmatrix} \tilde{V}_D^{\max} - \Gamma_{\mathrm{VD}} \\ \Gamma_{\mathrm{VD}} - \tilde{V}_D^{\min} \\ \tilde{E}^{\max} - \Gamma_E \\ \Gamma_E - \tilde{E}^{\min} \\ -\Gamma_B \\ \Gamma_{\mathrm{NS}m} \\ \tilde{P}_B^{\max} \\ \tilde{S}_L^{\max} \\ -\tilde{S}_L^{\min}(k) \\ 0 \\ 0 \\ 0 \\ 0 \end{bmatrix} \\
&\qquad\qquad\qquad\qquad\qquad\qquad m=1,\ldots,8 \qquad (39)
\end{aligned}$$

where $\|\bar{G}_i\widetilde{u}(k)\|_2 \le t$, $i=1,\ldots,N_p$, is the constraint coming from the original restriction $\tilde{P}_B^+(k)\cdot\tilde{P}_B^-(k)=0$.

It is worth pointing out that (q_m, r_m) are time variant. Such a variation obeys the dependence of these matrices on: 1) the membership functions used for modeling the consumption of diesel; 2) the maximum power demanded for the battery in charging mode; and 3) the behavior of the demand and the NCES. However, the parameters of the models are computed offline and therefore can be assumed known. Let $A_{\mathrm{des}m}$ and $b_{\mathrm{des}m}$ denote the matrices associated with the linear constraints in (39). Then assuming that the parameters of the models are known, the following steps are suggested for implementing the proposed robust EMS.

1) Given the current operating point, determine the membership functions $\beta_{Sj}(x_{pS}(k))$, $\beta_{Ej}(x_{pE}(k))$, and $\beta_{Lj}(x_{pL}(k))$ of the different models.
2) With the membership functions, determine the free and forced responses of the conventional energy sources.
3) With the membership functions, determine upper and lower boundaries for the free and forced responses of the NCES and of the demand.
4) Define the values for q and r as well as the values for $A_{\mathrm{des}m}$ and $b_{\mathrm{des}m}$.
5) Compute the optimal control sequence $\widetilde{u}^*(k)$ as the solution of (39).
6) Apply the first element of $\widetilde{u}(k)$ and define the initial condition for the next time step as $u_o(k+1) = \widetilde{u}(k)^{*T}$ (the superscript $*$ denotes the optimal solution).
7) Go back to Step 1.

Note that the minimization problem (39) is a convex optimization problem. Then, it is possible to guarantee that the solution converges to the global minimum. In fact, efficient procedures have been proposed for solving such a kind of optimization problems. In Section IV, the proposed robust EMS is tested through simulation in the Huatacondo microgrid.

IV. CASE STUDY

With the aim of evaluating the performance of the proposed robust EMS, the microgrid installed in Huatacondo, Chile, was used as a test bench. Huatacondo is a human settlement located in the Atacama Desert. In this village, an isolated microgrid was implemented in order to provide 24 h of electricity to its inhabitants, instead of the 10-h electricity, they previously had with only a diesel generator. The idea behind implementing the microgrid was taking advantage of the distributed NCES in the area for supplying the energy demanded by the community. Thereby, a photovoltaic system with a maximum capacity of $P_{\mathrm{Smax}} = 22$ kW, a wind generator system rated at $P_{\mathrm{Emax}} = 5$ kW, and an ESS (connected to the grid through a power inverter) were implemented to complement the existing diesel generator, which has a $P_{\mathrm{Dmax}} = 120$ kW. The demand of Huatacondo is composed by a water pump (used as a programmable load), the inhabitant's power consumption, and the street lights. Combining all consumption the maximum demand P_{Lmax} is about 28 kW.

In Huatacondo, the energy sources are coordinated by means of an EMS. The EMS is in charge of defining the power references for the diesel generator and the battery bank. In addition, the EMS defines when and how long the controllable loads are fed. Fig. 1 shows a block diagram of the EMS installed in Huatacondo. In that EMS, the inputs are: 1) the SoC of the battery bank; 2) the weather conditions (sunlight and wind speed mainly); and 3) the expected values of both the demand and the water consumption.

Moreover, the weather conditions (and therefore the available energy in the NCES) and the demand are estimated using historical data. These estimations do not consider the uncertainty. Therefore, the reliability of the microgrid cannot be assured. Based on the scheme shown in Fig. 1, and with the aim of enhancing the reliability of the microgrid, the proposed robust EMS has been implemented. In the implementation, requirements such as: 1) a prediction horizon of two days

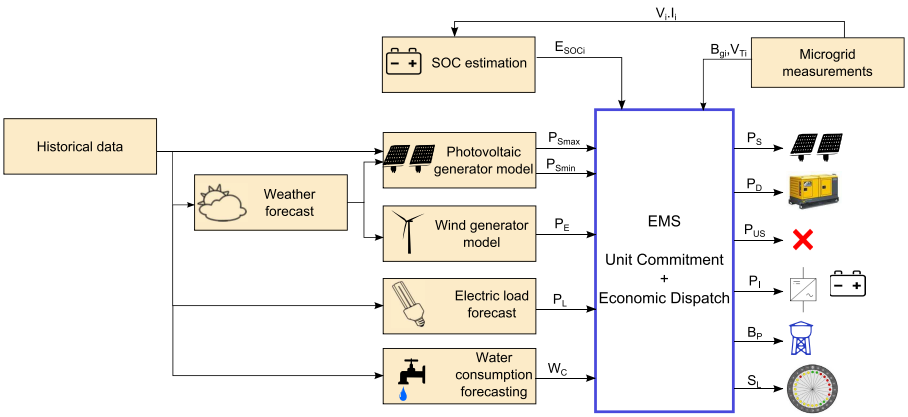

Fig. 1. Block diagram of the EMS installed in the microgrid of Huatacondo.

for the demand, the wind-based, and the solar-based power; 2) generating the power references for the diesel and the battery bank; 3) providing the load shifting signals to the community; and 4) a sampling time of 15 min were considered. In the following sections, the models used and the results obtained in the implementation are presented. Furthermore, a comparison between the EMS and its robust version is included. The comparison is done considering the operating costs as the comparison index. In this paper, three robust EMSs arising from Table I are compared, namely, the worst case scenario that corresponds to scenario 4 in Table I, a case in which scenarios 3 and 7 are considered (here only uncertainty in the load forecasting is assumed), and a case in which all scenarios are taken into account. In all the cases, the EMS installed in Huatacondo was modified in order to solve (39) considering the prediction conditions associated with each EMS.

A. INFUMO for Demand, Solar Generation, and Wind Generation in Huatacondo

In the proposed robust EMS, the identification of INFUMO for the load, solar power, and wind power is required. These are the main sources of uncertainty in the microgrid installed in Huatacondo. Historical data of solar power, wind power, and load measured in Huatacondo were used to identify the INFUMO. Only in the case of the demand, exogenous variables were not considered in the model. The reason for this model selection was the independence of the load with respect to external factors, such as weather conditions. In addition to the parameter identification, the theorem in [35] and [36] was used to verify the stability of the models. The stability was verified to guarantee the same confidence level throughout the prediction horizon. If the confidence level enlarges due to the instability of one of the boundaries of the interval, then unfeasible references for the units might arise steering the system to undesirable operating conditions. Since the microgrid of Huatacondo provides energy to the inhabitants of the settlement, having an undesirable and/or unexpected behavior is not an option. Fig. 2(a)–(c) shows the INFUMO obtained for the demand, the available solar-based power, and the available wind-based power, respectively. The INFUMOs in Fig. 2 are obtained with the procedure described in Section II-B. In these models, a confidence level of 95% is accomplished. Moreover, the region defined by the INFUMO is wider enough to represent the information contained in the data. Thus, the INFUMO captured both the dynamics and the uncertainty present in the data used in the parameter identification procedure. Fig. 2(a)–(c) shows a comparison between the real data and the INFUMO. In Fig. 2(a)–(c), the validation data set is presented. The capabilities of the INFUMO are more evident in the demand and wind-based generation, since the variability of these variables is higher than the variability of the solar-based generation. Those differences obey the conditions of the Atacama Desert, where the radiation is almost the same the whole year and the operating mode of the microgrid. Since the microgrid is operating in isolated mode, any change in the consumption pattern of the inhabitants has a notorious impact in the measured load.

B. Worst Case Scenario

For comparison purposes, in this paper, the worst case scenario is also considered. From Table I, the worst case corresponds to the prediction scenario 4. In this scenario, the expected demand is high (represented by the upper boundary of the INFUMO), but the expected available energy in the NCES is low (represented by the lower boundary of the INFUMO of both energy sources). The comparison seeks to demonstrate that a high variability in the operating costs is obtained when the same prediction scenario is considered in the EMS, as it is explained in Section IV-D. Fig. 3 shows the operation of the microgrid when the worst case scenario is used in the EMS.

As it can be observed in Fig. 3, the operating conditions of the selected days are very diverse. The more notorious difference lies in the load profile. The changes in the load cause the EMS to use the battery bank to produce the expected missing energy. Due to the intense use of the battery bank, its minimum (allowed) energy value is reached several times. Thus, a reduction of the lifespan of the battery bank is expected, and therefore, an increasing in the investment since the replacement of the banks should be scheduled more often than planned. In addition, the use of the diesel

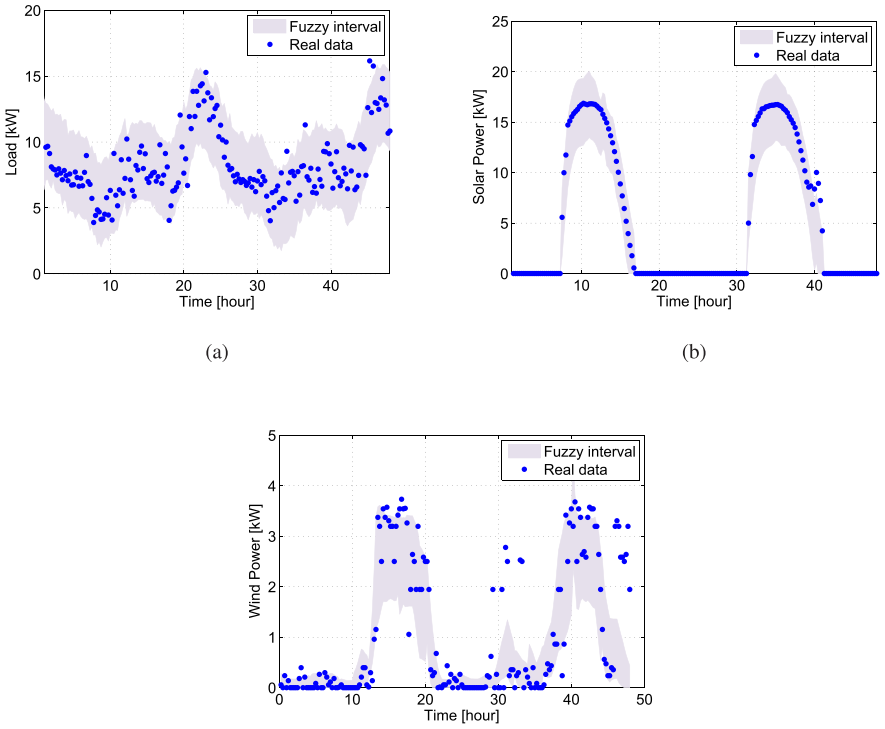

Fig. 2. INFUMOs for the demand, for the photovoltaic generation, and for the wind-based generation in the microgrid of Huatacondo. (a) 95% of confidence level INFUMO for the demand. (b) 95% of confidence level INFUMO for the photovoltaic power. (c) 95% of confidence level INFUMO for the wind-based power.

generator increases. Indeed, Fig. 3(d) shows a case in which the EMS started two times the diesel generator. This also increases the operating costs of the microgrid. Remember that Huatacondo is an isolated place in the Atacama Desert, and therefore, carrying the diesel to this place is a very expensive task.

With respect to the cost function, notwithstanding the intensive use of the battery bank, its value is not severely affected since the operating conditions of the diesel generator do not change very often. Indeed, only the second day exhibits a considerable variation in the operating costs, as it can be validated in Table II. The difference obeys the amount of diesel used during this day. As shown in Fig. 3(b), the diesel generator was started and remained providing the total demanded energy during a long period, before being turned OFF by the EMS. Given these results, it can be concluded that the use of a single scenario in the EMS might threaten the security and reliability of the microgrid. This motivates even more the use of the robust EMS proposed in this paper.

C. Proposed Robust EMS: Load Uncertainty

In this section, the results obtained considering uncertainty only in the load forecasting are presented. In this case, the prediction scenarios 3 and 7 of Table I are selected. These prediction scenarios provide an upper and a lower boundary for the prediction of the load. The reason for selecting these scenarios is that, as in scenario 4, the prediction of the solar power is performed through the lower boundary model. Thus, the effect of taking into consideration the uncertainty in the EMS can be evaluated by comparing the results obtained with both prediction scenarios (worst case and load uncertainty). Note that in scenarios 3 and 7, the wind power is predicted assuming the upper boundary of the interval, while in scenario 4, the same prediction is performed using the lower boundary. However, since the wind power is significantly less than the solar power (during the experiments), the effects of the variations in the prediction scenario were neglected.

Fig. 4 shows the results obtained with the implementation of the proposed robust EMS. In Fig. 4, despite the variability in the demand the use of the diesel generator remained almost the same. Nevertheless, the use of the battery bank significantly changed from one day to another. These changes

TABLE II
OPERATING COSTS FOR THE WORST CASE SCENARIO

Day:	Operating Costs	Start Up Costs	Total Costs
1	10350	2000	12350
2	24252	1000	25252
3	12727	1000	13727
4	14156	2000	16156

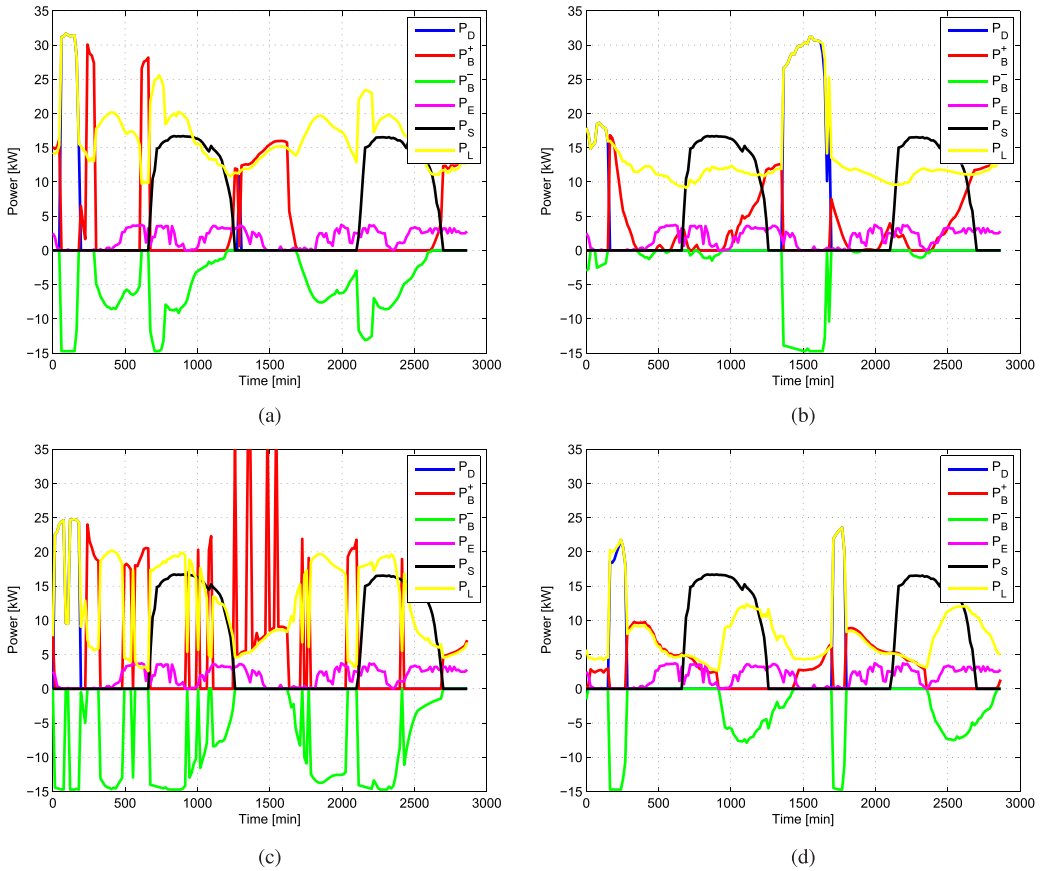

Fig. 3. Performance of the Huatacondo microgrid. Here, the worst case scenario for the predictions was considered. Several load conditions were used to assess the performance of the microgrid. (a) Performance of the microgrid in a type 1 day when the forecasting scenario is assumed the worst ($m = 4$). (b) Performance of the microgrid in a type 2 day when the forecasting scenario is assumed the worst ($m = 4$). (c) Performance of the microgrid in a type 3 day when the forecasting scenario is assumed the worst ($m = 4$). (d) Performance of the microgrid in a type 4 day when the forecasting scenario is assumed the worst ($m = 4$).

are associated with the use of the battery and the diesel generator as reserves. Thus, the variability of the NCES and the load and their effects in the operation of the microgrid are mitigated. In comparison with the results shown in Fig. 3, including the scenarios produced a change in the way the EMS scheduled the use of the battery. Indeed, both the maximum charging and discharging powers are significantly diminished. Therefore, in comparison with the worst case scenario, the lifespan of the battery is increased. This fact is important because if the battery life is extended, the investment associated with maintenance and replacement could be decreased.

However, from the cost function proposed in [4], the use of scenarios to represent the uncertainty increases the operating costs. Table III summarizes the operating costs associated with the EMS in [4], with the worst case scenario EMS, and with the proposed robust EMS bearing in mind only the uncertainty in the load forecasting. As it can be noted, the use of several scenarios allowed maintaining the same operating costs for all days. Thereby, in the Huatacondo case, it is evidenced that the proposed EMS adequately dealt with the uncertainty. Indeed, it is validated the fact that robust programming provides solutions that are robust against any realization of the uncertain variable inside the range defined by the interval model (in this case by the INFUMO), since all the cases shown in Fig. 4 are defined by particular realizations of the load.

D. Proposed Robust EMS Considering Uncertainty in Load, Solar Power, and Wind Power Forecasting

In this section, the results obtained with the robust EMS are presented. In this case, unlike in Section IV-C, uncertainty in the load, solar power, and wind power forecasting were considered. Hence, given the measured values in the microgrid, the cases presented in Table I were computed. Afterward, the solution of (39) was obtained following the steps proposed in Section III-C. Similar to Section IV-C, analogous operating conditions to the used in the assessment of the worst case scenario EMS were considered. In this sense, the results obtained are comparable with each other.

Fig. 5 shows the results obtained with the proposed robust EMS. According to the results presented in Fig. 4, considering all scenarios in Table I allowed improving the use of the battery bank. Indeed, in this case, the maximum power taken from the battery bank is 5 kW, while in the worst case scenario is 35 kW and in the load uncertainty case is 20 kW. Furthermore, in the case of the robust EMS, a shallower discharge of the battery is obtained than in the previous cases.

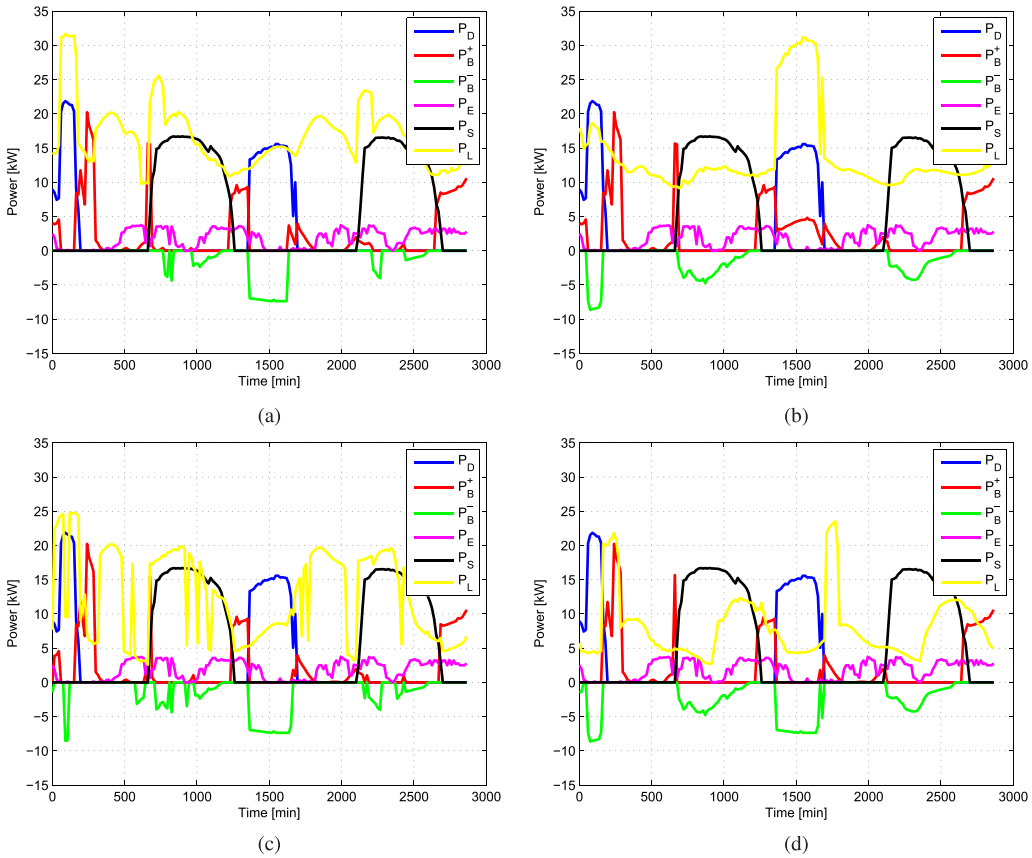

Fig. 4. Performance of the Huatacondo microgrid when the scenario-based robust EMS coordinates the energy sources at different days of operation. Here, only uncertainty in the load forecasting is considered. (a) Performance of the microgrid in a type 1 day. Here, the coordination of the energy sources is carried out by the scenario-based robust EMS. (b) Performance of the microgrid in a type 2 day. Here, the coordination of the energy sources is carried out by the scenario-based robust EMS. (c) Performance of the microgrid in a type 3 day. Here, the coordination of the energy sources is carried out by the scenario-based robust EMS. (d) Performance of the microgrid in a type 4 day. Here, the coordination of the energy sources is carried out by the scenario-based robust EMS.

TABLE III

COMPARISON OF THE OPERATING COSTS FOR THE SAME PREDICTION SCENARIO UNDER DIFFERENT OPERATING CONDITIONS. REMS STANDS FOR THE EMS DESCRIBED IN THIS PAPER, WC-EMS STANDS FOR THE EMS BASED ON THE WORST CASE SCENARIO, AND EMS STANDS FOR THE EMS PROPOSED IN [4]. HERE, ONLY UNCERTAINTY IN THE LOAD PREDICTIONS IS CONSIDERED

	Operating Costs (per day)				Start Up Costs (per day)				Total Costs (per day)			
	D1	D2	D3	D4	D1	D2	D3	D4	D1	D2	D3	D4
Strategy:												
REMS	17541	17541	17541	17541	2000	2000	2000	2000	19541	19541	19541	19541
WC-EMS	10350	24252	12727	14156	2000	1000	1000	2000	12350	25252	13727	16156
EMS	33070	36872	36780	32731	4000	3000	3000	3000	37070	39872	39780	35731

This is evidenced by the power required for charging the battery. In the worst case, for instance, the maximum power required for charging the battery is 15 kW, but in the load uncertainty and the current case, less than 10 kW is required. As it was aforementioned in Section IV-C, since the battery bank is used as an energy reserve, the depth in the battery discharge is reduced. Thus, any energy surplus is used to charge the battery bank. Consequently, the battery drain is diminished enlarging its lifespan.

Although the proposed EMS allows achieving the desired operating conditions in the microgrid, the use of the diesel must be slightly improved. For instance, fast changes in the power supplied by the diesel should be prevented (Fig. 5). These changes appear because the robust EMS uses the diesel generator as a spinning reserve to counteract the uncertainty in the NCES, despite the increasing in the operating costs. The operating costs associated with the EMS in [4], the worst case scenario EMS, and the robust EMS are summarized in Table IV. As expected, the EMS presents the highest operating costs. This is explained by the inaccuracy in the predictions of the uncertain variables. Also, it is evident that, in almost all the cases, the proposed EMS has higher operating costs

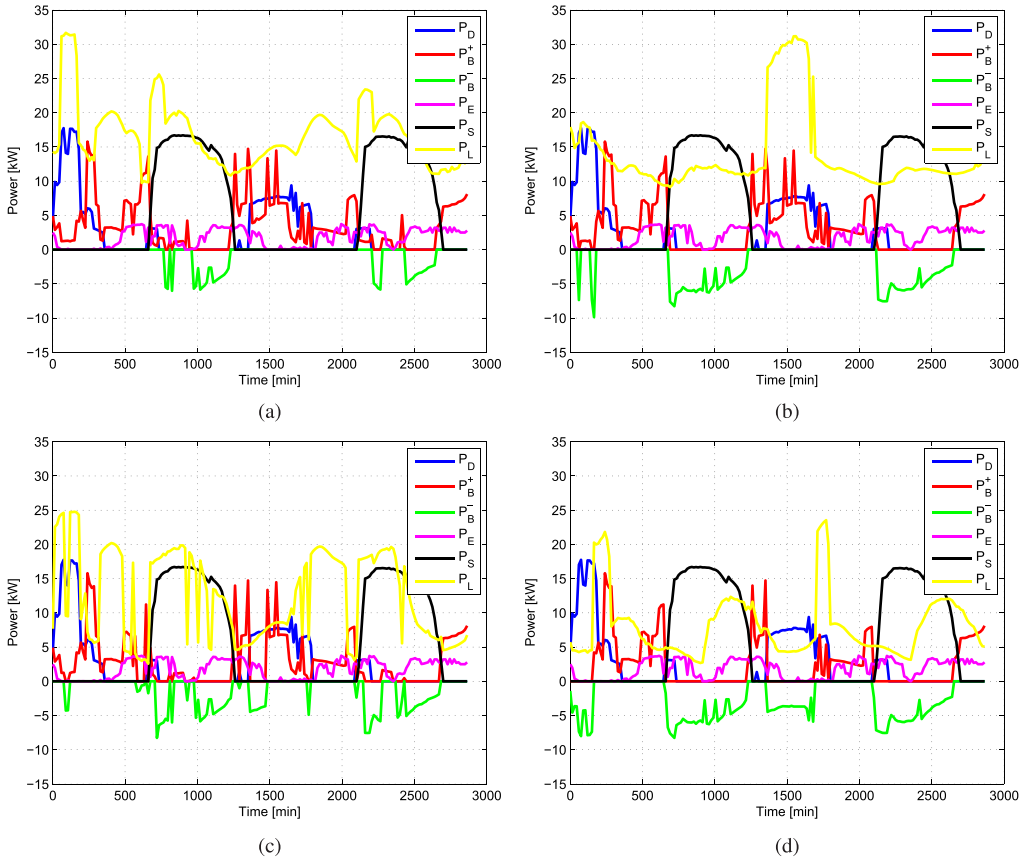

Fig. 5. Performance of the Huatacondo microgrid, when the scenario-based robust EMS coordinates the energy sources at different days of operation. Here, uncertainty in the load, the solar power, and the wind power forecasting is considered. (a) Performance of the microgrid in a type 1 day. Here, the coordination of the energy sources is carried out by the scenario-based robust EMS. (b) Performance of the microgrid in a type 2 day. Here, the coordination of the energy sources is carried out by the scenario-based robust EMS. (c) Performance of the microgrid in a type 3 day. Here, the coordination of the energy sources is carried out by the scenario-based robust EMS. (d) Performance of the microgrid in a type 4 day. Here, the coordination of the energy sources is carried out by the scenario-based robust EMS.

TABLE IV

COMPARISON OF THE OPERATING COSTS FOR THE SAME PREDICTION SCENARIO UNDER DIFFERENT OPERATING CONDITIONS. REMS STANDS FOR THE EMS DESCRIBED IN THIS PAPER, WC-EMS STANDS FOR THE EMS BASED ON THE WORST CASE SCENARIO, AND EMS STANDS FOR THE EMS PROPOSED IN [4]. HERE, IT IS ASSUMED UNCERTAINTY IN THE NCES AND IN THE LOAD FORECASTING

	Operating Costs (per day)				Start Up Costs (per day)				Total Costs (per day)			
	D1	D2	D3	D4	D1	D2	D3	D4	D1	D2	D3	D4
Strategy:												
REMS	16937	18675	17234	17413	2000	2000	2000	2000	18937	20675	19234	19413
WC-EMS	10350	24252	12727	14156	2000	1000	1000	2000	12350	25252	13727	16156
EMS	33070	36872	36780	32731	4000	3000	3000	3000	37070	39872	39780	35731

than in the worst case scenario. This result is mainly because, as aforementioned, the robust EMS uses the diesel generator as spinning reserve. However, in comparison with the results presented in Table III, including more scenarios allowed diminishing the operating costs. Only in the second day, the robust EMS with uncertainty in the load forecasting performed better than the EMS analyzed in this section. Nonetheless, the operating costs remained almost the same despite the changes in the operating conditions. Therefore, the proposed EMS is an adequate alternative to address the uncertainty in the coordination of energy sources in a microgrid.

V. CONCLUSION

In this paper, a scenario-based robust EMS was proposed for coordinating the energy resources in an isolated microgrid. The proposed EMS was formulated within the MPC framework. Fuzzy prediction models were used to represent the system dynamics. Specifically, TS models were considered.

The selection of these models allowed deriving recursive expressions to compute the predictions in an efficient way. Thus, only the current measured values of the states and outputs of the system are required to compute the optimal control actions. This fact significantly reduced the computational burden of the proposed EMS.

Notwithstanding the capabilities of TS models, in microgrids, there are several uncertainties that these models are not able to represent. Therefore, instead of using directly TS models, in this paper, they were used as the basis to formulate INFUMOs of the uncertain variables. The fuzzy interval models provided upper and lower boundaries for the trajectories of the uncertain variables. Thereby, within the range delimited by these boundaries, any realization of the uncertain variables was represented by the interval model. The range covered by the model depends on the desired confidence level. Thus, both the dynamic behavior of the microgrid and its uncertainty were represented.

Taking into consideration the boundaries provided by the INFUMOs, several feasible scenarios were generated. In fact, the scenarios considered here corresponded to all combinations of the extreme cases of the interval models, e.g., considering the prediction using the upper boundary model of the NCES and prediction using the lower boundary model of the load determined one of the scenarios. Considering all possible scenarios, the robust EMS was initially formulated as a robust programming problem, and then, it was transformed into an SOCP problem. In this sense, efficient algorithms were available to solve the robust EMS problem. Furthermore, since SOCP problems are convex, their solution is obtained in a finite number of steps, and the convergence of the solution to the global optimum might be demonstrated.

Although the problem of uncertainty in microgrids and, in general, in power systems with NCES has been widely investigated in the literature, several approaches are based on the Monte Carlo simulation or in the use of probability functions to generate the scenarios. In these approaches, the solution is robust only against the realizations included in the solution. By contrast, with the use of interval modeling plus robust programming, the solution is robust against all possible realizations, within the interval, of the uncertain variables. In the literature, several approaches using fixed intervals or intervals whose width changes according to the prediction error for representing the uncertainty have been reported. In comparison with these approaches, in this paper, the use of fuzzy interval models for changing the boundaries of the interval in accordance with the system dynamics is investigated. The intervals have been associated with a confidence level. The confidence level determines the width of the interval and therefore the degree of representation of the uncertain variables. Since the boundaries are adapted in accordance with the system dynamics, the proposed EMS provides less conservative solutions.

The assessment of the robust EMS was carried out using the microgrid installed in Huatacondo. For comparison purposes, the currently installed one and an EMS based on the worst case scenario were considered. The comparison was done using the operating costs as a comparison index. With respect to the currently installed, the robust EMS performed better. Specifically, the operating costs were reduced, and the security and reliability were improved. In comparison with the worst case scenario, the robust EMS provided a better use of the battery and the costs remained almost constant despite the changes in the operating conditions. However, since the diesel generator was used as spinning reserve, the operating costs (in terms of the cost function of the EMS) were higher than in the worst case scenario, in almost all the cases analyzed. Therefore, it was concluded that the proposed robust EMS adequately addressed the uncertainty in the Huatacondo microgrid.

REFERENCES

[1] R. H. Lasseter, "MicroGrids," in *Proc. IEEE Power Eng. Soc. Winter Meeting*, vol. 1. Jan. 2002, pp. 305–308.

[2] J. M. Guerrero, J. C. Vasquez, J. Matas, L. G. de Vicuña, and M. Castilla, "Hierarchical control of droop-controlled AC and DC microgrids—A general approach toward standardization," *IEEE Trans. Ind. Electron.*, vol. 58, no. 1, pp. 158–172, Jan. 2011.

[3] B. Wright. (2013). *A Review of Unit Commitment*. [Online]. Available: http://www.ee.columbia.edu/ lavaei/Projects/Brittany_Wright.pdf

[4] R. Palma-Behnke *et al.*, "A microgrid energy management system based on the rolling horizon strategy," *IEEE Trans. Smart Grid*, vol. 4, no. 2, pp. 996–1006, Jun. 2013.

[5] Y. Zhang, N. Gatsis, and G. B. Giannakis, "Robust energy management for microgrids with high-penetration renewables," *IEEE Trans. Sustainable Energy*, vol. 4, no. 4, pp. 944–953, Oct. 2013.

[6] S. Wang, G. H. Huang, and B. T. Yang, "An interval-valued fuzzy-stochastic programming approach and its application to municipal solid waste management," *Environ. Model. Softw.*, vol. 29, no. 1, pp. 24–36, 2012. [Online]. Available: http://www.sciencedirect.com/science/article/pii/S1364815211002180

[7] D. Bertsimas, E. Litvinov, X. A. Sun, J. Zhao, and T. Zheng, "Adaptive robust optimization for the security constrained unit commitment problem," *IEEE Trans. Power Syst.*, vol. 28, no. 1, pp. 52–63, Feb. 2013.

[8] S. Wang and G. H. Huang, "An interval-parameter two-stage stochastic fuzzy program with type-2 membership functions: An application to water resources management," *Stochastic Environ. Res. Risk Assessment*, vol. 27, no. 6, pp. 1493–1506, 2013. [Online]. Available: http://dx.doi.org/10.1007/s00477-013-0685-2

[9] S. Wang and G. H. Huang, "A two-stage mixed-integer fuzzy programming with interval-valued membership functions approach for flood-diversion planning," *J. Environ. Manage.*, vol. 117, pp. 208–218, Mar. 2013. [Online]. Available: http://www.sciencedirect.com/science/article/pii/S0301479713000078

[10] X. H. Nie, G. H. Huang, Y. P. Li, and L. Liu, "IFRP: A hybrid interval-parameter fuzzy robust programming approach for waste management planning under uncertainty," *J. Environ. Manage.*, vol. 84, no. 1, pp. 1–11, 2007. [Online]. Available: http://www.sciencedirect.com/science/article/pii/S0301479706001356

[11] S. P. Boyd, L. Vandenberghe, and M. Grant, "Efficient convex optimization for engineering design," in *Proc. IFAC Symp. Robust Control Design*, 1994, pp. 14–23.

[12] C. Zhao, J. Wang, J.-P. Watson, and Y. Guan, "Multi-stage robust unit commitment considering wind and demand response uncertainties," *IEEE Trans. Power Syst.*, vol. 28, no. 3, pp. 2708–2717, Aug. 2013.

[13] Z. Yu, L. McLaughlin, L. Jia, M. C. Murphy-Hoye, A. Pratt, and L. Tong, "Modeling and stochastic control for home energy management," in *Proc. IEEE Power Energy Soc. General Meeting*, Jul. 2012, pp. 1–9.

[14] A. Parisio and L. Glielmo, "Energy efficient microgrid management using model predictive control," in *Proc. 50th IEEE Conf. Decision Control, Eur. Control Conf. (CDC-ECC)*, Dec. 2011, pp. 5449–5454.

[15] B. Zhao, Y. Shi, X. Dong, W. Luan, and J. Bornemann, "Short-term operation scheduling in renewable-powered microgrids: A duality-based approach," *IEEE Trans. Sustainable Energy*, vol. 5, no. 1, pp. 209–217, Jan. 2014.

[16] P. Pinson and G. Kariniotakis, "Conditional prediction intervals of wind power generation," *IEEE Trans. Power Syst.*, vol. 25, no. 4, pp. 1845–1856, Nov. 2010.

[17] I. Škrjanc, S. Blažič, and O. Agamennoni, "Identification of dynamical systems with a robust interval fuzzy model," *Automatica*, vol. 41, no. 2, pp. 327–332, 2005.
[18] S. Boyd and L. Vandenberghe, *Convex Optimization*. Cambridge, U.K.: Cambridge Univ. Press, 2004.
[19] P. O. M. Scokaert, J. B. Rawlings, and E. S. Meadows, "Discrete-time stability with perturbations: Application to model predictive control," *Automatica*, vol. 33, no. 3, pp. 463–470, 1997.
[20] J. H. Lee and Z. Yu, "Worst-case formulations of model predictive control for systems with bounded parameters," *Automatica*, vol. 33, no. 5, pp. 763–781, 1997.
[21] G. Pannocchia, "Robust model predictive control with guaranteed setpoint tracking," *J. Process Control*, vol. 14, no. 8, pp. 927–937, 2004.
[22] D. Limon, I. Alvarado, T. Alamo, and E. F. Camacho, "Robust tube-based MPC for tracking of constrained linear systems with additive disturbances," *J. Process Control*, vol. 20, no. 3, pp. 248–260, 2010.
[23] W. Al-Gherwi, H. Budman, and A. Elkamel, "A robust distributed model predictive control algorithm," *J. Process Control*, vol. 21, no. 8, pp. 1127–1137, 2011.
[24] J. Espinosa, J. Vandewalle, and V. Wertz, *Fuzzy Logic, Identification and Predictive Control*. London, U.K.: Springer-Verlag, 2005.
[25] J. Espinosa and J. Vandewalle, "Nonlinear predictive control using fuzzy models and semidefinite programming," in *Proc. 18th Int. Conf. North Amer. Fuzzy Inf. Process. Soc. (NAFIPS)*, Jul. 1999, pp. 174–178.
[26] M. B. Gorzałczany, "A method of inference in approximate reasoning based on interval-valued fuzzy sets," *Fuzzy Sets Syst.*, vol. 21, no. 1, pp. 1–17, 1987.
[27] G. Wang and X. Li, "The applications of interval-valued fuzzy numbers and interval-distribution numbers," *Fuzzy Sets Syst.*, vol. 98, no. 3, pp. 331–335, 1998.
[28] I. B. Turksen, "Interval valued fuzzy sets based on normal forms," *Fuzzy Sets Syst.*, vol. 20, no. 2, pp. 191–210, 1986.
[29] A. Núñez and B. De Schutter, "Distributed identification of fuzzy confidence intervals for traffic measurements," in *Proc. 51st IEEE Conf. Decision Control*, Maui, HI, USA, Dec. 2012, pp. 6995–7000.
[30] T. Takagi and M. Sugeno, "Fuzzy identification of systems and its applications to modeling and control," *IEEE Trans. Syst., Man, Cybern.*, vol. SMC-15, no. 1, pp. 116–132, Jan./Feb. 1985.
[31] P. Pinson, H. Madsen, H. A. Nielsen, G. Papaefthymiou, and B. Klöckl, "From probabilistic forecasts to statistical scenarios of short-term wind power production," *Wind Energy*, vol. 12, no. 1, pp. 51–62, 2009.
[32] J. Michalakes *et al.*, "Development of a next generation regional weather research and forecast model," in *Proc. 9th ECMWF Workshop High Perform. Comput. Meteorol., Develop. Teracomput.*, vol. 1. 2001, pp. 269–276.
[33] J. Michalakes *et al.*, "The weather research and forecast model: Software architecture and performance," in *Proc. 11th ECMWF Workshop High Perform. Comput. Meteorol.*, vol. 25. Reading, U.K. 2004, p. 29.
[34] V. M. Zavala, E. M. Constantinescu, and M. Anitescu, "Economic impacts of advanced weather forecasting on energy system operations," in *Proc. Innov. Smart Grid Technol. (ISGT)*, 2010, pp. 1–7.
[35] K. Tanaka and M. Sugeno, "Stability analysis and design of fuzzy control systems," *Fuzzy Sets Syst.*, vol. 45, no. 2, pp. 135–156, 1992.
[36] F. Ávila, D. Sáez, G. Jiménez-Estévez, L. Reyes, and A. Núñez, "Fuzzy demand forecasting in a predictive control strategy for a renewable-energy based microgrid," in *Proc. Eur. Control Conf. (ECC)*, Jul. 2013, pp. 2020–2025.

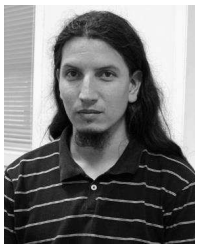

Felipe Valencia (M'13) was born in Medellín, Colombia. He received the master's and Ph.D. (*magna cum laude*) degrees in control engineering from the Universidad Nacional de Colombia, Medellín.

He is currently a full-time Researcher with the Department of Electrical Engineering, Solar Energy Research Center, Universidad de Chile, Santiago. He has been involved in different fields, such as power energy generation, transmission, and distribution systems; transportation; and smart grids. His current research interests include design of distributed and hierarchical strategies for controlling large-scale systems.

Doris Sáez was born in Paguipulli, Chile. He received the M.Sc. and Ph.D. degrees in electrical engineering from the Pontificia Universidad Católica de Chile, Santiago, in 1995 and 2000, respectively.

She is currently an Associate Professor with the Department of Electrical Engineering, Universidad de Chile, Santiago. She has co-authored the books entitled *Hybrid Predictive Control for Dynamic Transport Problems* (Springer-Verlag, 2013) and *Optimization of Industrial Processes at Supervisory Level: Application to Control of Thermal Power Plants* (Springer-Verlag, 2002). Her current research interests include predictive control, fuzzy control design, fuzzy identification, control of power generation plants, and control of transport systems.

Dr. Sáez is an Associate Editor of the IEEE TRANSACTIONS ON FUZZY SYSTEMS.

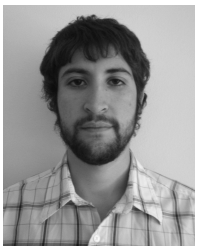

Jorge Collado was born in Santiago, Chile. He received the B.Sc. degree in electrical engineering from the Universidad de Chile, Santiago, in 2013.

His current research interests include robust energy management systems and microgrids.

Fernanda Ávila was born in Santiago, Chile. She received the B.Sc. and M.Sc. degrees in electrical engineering from the Universidad de Chile, Santiago, in 2011 and 2013, respectively.

Her current research interests include fuzzy systems and renewable energy plants.

Alejandro Marquez was born in Medellín, Colombia. He received the B.S. degree in control engineering and the M.S. degree in chemical engineering from the Universidad Nacional de Colombia, Medellín, Colombia, in 2008 and 2010, respectively, where he is currently pursuing the Ph.D. degree in energy systems engineering.

His current research interests include robust hierarchical model predictive control, model reduction techniques, and large-scale systems.

Jairo J. Espinosa (SM'06) was born in Bogotá, Colombia. He received the Electronics Engineering degree from the Universidad Distrital de Bogotá, Bogotá, Colombia, and the master's (*cum laude*) and Ph.D. (*magna cum laude*) degrees in electrical engineering from the Katholieke Universiteit Leuven, Leuven, Belgium.

He was the Research and Development Manager with IPCOS N.V., Leuven, where he was involved in research on advanced process control systems. He has been involved in the creation of products to construct inferential sensors, nonlinear model-based predictive controllers, and process optimization. He has experience in many industrial areas, including oil, polymers, petrochemicals, automotive, power generation, and iron production, in which he has applied many of his developments. He is currently a Full Professor with the Universidad Nacional de Colombia at Medellín, Colombia. His current research interests include large-scale systems, intelligent control, mathematical modeling, model-based predictive control, inferential sensors, signal processing, optimization, and model reduction techniques.